Multibody Syst Dyn
DOI 10.1007/s11044-007-9049-3

An energy preserving/decaying scheme for nonlinearly constrained multibody systems

Elisabet Lens · Alberto Cardona

Received: 2 November 2005 / Accepted: 5 February 2007

Abstract Several numerical time integration methods for multibody system dynamics are described: an energy preserving scheme and three energy decaying ones, which introduce high-frequency numerical dissipation in order to annihilate the nondesired high-frequency oscillations. An exhaustive analysis of these four schemes is done, including their formulation, and energy preserving and decaying properties by taking into account the presence of nonlinear algebraic constraints and the incrementation of finite rotations. A new energy preserving/decaying scheme is developed, which is well suited for either stiff or nonstiff nonlinearly constrained multibody systems. Examples on a series of test cases show the performance of the algorithms.

Keywords Time integration · DAE systems · Nonlinear multibody systems dynamics · Energy preservation · Energy dissipation

1 Introduction

Integration of second-order index 3 Differential-Algebraic Equations (DAE) may lead to numerical instability when an integration method of the Newmark family is used, because of the algebraic constraints that are the cause of unbounded linearly growing oscillations in the acceleration response (weak instability). If a high-frequency dissipation is introduced, this instability can be controlled in the linear regime, e.g., using either HHT [1] or Hulbert α-generalized methods [2].

In the nonlinear regime, the stability cannot be guaranteed by usual methods of analysis that are based on the properties of the system amplification matrix. An alternative to ensure the stability of the solution is by means of schemes that verify the preservation of the total energy of the system at each time step. This discrete preservation of a positive amount over each time step ensures the algorithm unconditional stability in the nonlinear regime [3].

E. Lens · A. Cardona (✉)
Centro Internacional de Métodos Computacionales en Ingeniería, CIMEC-INTEC, Conicet-Universidad Nacional del Litoral, Güemes 3450, 3000 Santa Fe, Argentina
e-mail: acardona@intec.unl.edu.ar

Energy preserving methods were used for the first time in the context of the Finite-Element Method by Haug et al. [4] and Hughes et al. [5], where the preservation of the energy was enforced as a constraint by using Lagrange multipliers. These methods, termed *enforced preservation methods*, are not considered strictly as preserving or dissipative schemes: since the higher modes are dissipated while the total system energy must at the same time remain constant, these algorithms transfer energy from the higher to the lower modes, a process that is nonphysical [6].

Simo et al. [7–10] explored the idea of *midpoint equilibrium* that follows on from the work of Hilber et al. [11] and Zienkiewicz et al. [12], to introduce algorithms that preserve the total energy for unconstrained systems of rigid bodies, rods, nonlinear beams, and nonlinear elastodynamics. Ibrahimbegovic and Mamouri [13] have developed an energy conserving algorithm for flexible multibody systems with constraints. Betsch and Steinmann have proposed energy preserving schemes for N-body problems [14], nonlinear elastodynamics [15], mechanical systems with holonomic constraints [16], and dynamics of constrained rigid bodies [17], using a mixed Galerkin-based discretization method, a temporal counterpart of mixed finite-element methods in space.

Bauchau et al. [18] proposed an energy preserving scheme for flexible multibody systems where the equations are discretized so that they imply perfect preservation of the energy for the elastic parts of the system and guarantees that the work performed by the constraint forces associated with the kinematic constraints perfectly vanishes. The combination of these two features ensures the stability of the numerical integration process for nonlinear multibody flexible systems. Géradin [19] proposed an energy preserving scheme inspired in Bauchau's methodology, which was reviewed by the authors in an early work [20].

However, the unconditional stability of the energy preserving methods is not enough for obtaining a satisfactory performance of the scheme, because of the spurious high-frequency oscillations that may appear, e.g., with a sudden variation of stiffness or with shock, conserved all along the response masking the answer. For this reason, alternative schemes have been proposed. A methodology that leads to a systematic formulation of energy dissipative integration schemes is time-discontinuous Galerkin (TDG) [21], initially developed for hyperbolic equations. Bauchau et al. [18, 22, 23] proposed "practical" schemes constructed by using finite-difference schemes that imply an energy balance obtained directly from the computation of the work done by the inertia and elastic forces over a time step. This condition of energy balance is used to derive the requisites to obtain the preservation or dissipation of the energy. Armero and Romero [24, 25] proposed energy decaying algorithms for nonlinear elastodynamics without control of the asymptotic spectral radius. Ibrahimbegovic and Mamouri [26] developed a scheme as an extension of existing energy conserving schemes [10, 13, 27]. Recently, Bottasso and Trainelli [6] reviewed some of the temporal underlying schemes mentioned earlier, pointing out differences and similarities between them.

In this work, a systematic way for formulating a dissipative integration scheme is proposed with the following features: (i) unconditionally stable integration in constrained nonlinear elastodynamics, (ii) energy dissipation with control of the asymptotic spectral radius, (iii) capability of handling nonlinear constraints, (iv) capability of handling large finite rotations, and (v) continuous variation of the asymptotic spectral radius varying from energy preservation up to total annihilation. All these features are of utmost importance for the good performance of a time integration algorithm in flexible multibody dynamics, and are not verified by most of the algorithms mentioned earlier.

The paper is organized as follows: in Section 2, the problem is formulated. In Section 4, the energy preserving scheme studied in [20] is reformulated, by using the time-continuous Galerkin approximation. Based on the same methodology, dissipative schemes are developed

by using the time-discontinuous Galerkin approximation. Several algorithms are developed and analyzed all along Section 5 by comparing their performances for a set of test cases. Section 3 describes these nonlinear dynamics tests which were designed to highlight the merits and failures of each algorithm: (i) a nonstiff case without constraints, (ii) a nonstiff case with nonlinear constraints, and (iii) a stiff case with nonlinear constraints. Conclusions and future work are given in Section 6.

2 Formulation of the problem

Let us describe a conservative mechanical system in terms of N generalized coordinates $\boldsymbol{q}$ submitted to R algebraic constraints

$$\boldsymbol{\Phi}(\boldsymbol{q}) = \boldsymbol{0}. \tag{1}$$

Its dynamic properties can be derived from an appropriate description of the potential energy of the system $\mathcal{V} = \mathcal{V}(\boldsymbol{q})$ and of its kinetic energy, which can be put in a quadratic form without loss of generality

$$\mathcal{K} = \frac{1}{2}\boldsymbol{v}^{\mathrm{T}}\boldsymbol{M}\boldsymbol{v}. \tag{2}$$

The $(M \times M)$ inertia matrix $\boldsymbol{M}$ can be assumed constant, symmetric, and positive definite since velocities $\boldsymbol{v}$ are expressed in a *material frame*. The latter are treated as quasicoordinates and thus take the form of linear combinations of generalized coordinate time derivatives

$$\boldsymbol{v} = \boldsymbol{L}(\boldsymbol{q})\dot{\boldsymbol{q}}, \tag{3}$$

$\boldsymbol{L}(\boldsymbol{q})$ being a $(M \times N)$ matrix with $M \leq N$. This inequality covers the case in which the description of angular velocities is made in terms of redundant rotation parameters such as Euler parameters. In this case, the redundancy between parameters has to be removed by adding appropriate constraints to the global set (1).

The motion equations result from the application of Hamilton's principle:

$$\delta \int_{t_1}^{t_2} \left\{ \frac{1}{2}\boldsymbol{v}^{\mathrm{T}}\boldsymbol{M}\boldsymbol{v} - \boldsymbol{\mu}^{\mathrm{T}}(\boldsymbol{v} - \boldsymbol{L}(\boldsymbol{q})\dot{\boldsymbol{q}}) - \mathcal{V}(\boldsymbol{q}) - \boldsymbol{\lambda}^{\mathrm{T}}\boldsymbol{\Phi}(\boldsymbol{q}) \right\} dt = 0. \tag{4}$$

By performing successive variations on the variables $\boldsymbol{\mu}$, $\boldsymbol{\lambda}$, $\boldsymbol{v}$, and $\boldsymbol{q}$:

- the variation of the multipliers $\boldsymbol{\mu}$ restores the velocity Equations (3)
- variation of the multipliers $\boldsymbol{\lambda}$ restores the constraints set (1)
- the variation of the velocities $\boldsymbol{v}$ shows that the multipliers $\boldsymbol{\mu}$ have the meaning of generalized momenta

$$\boldsymbol{\mu} = \boldsymbol{M}\boldsymbol{v} \tag{5}$$

- the variation of the generalized displacements $\boldsymbol{q}$ yields

$$\int_{t_1}^{t_2} \left\{ \delta\boldsymbol{q}^{\mathrm{T}} \left(-\frac{\partial \mathcal{V}}{\partial \boldsymbol{q}} - \frac{\partial \boldsymbol{\Phi}^{\mathrm{T}}}{\partial \boldsymbol{q}}\boldsymbol{\lambda} + \frac{\partial}{\partial \boldsymbol{q}}[(\boldsymbol{L}\dot{\boldsymbol{q}})^{\mathrm{T}}\boldsymbol{\mu}] \right) + \delta\dot{\boldsymbol{q}}^{\mathrm{T}}\boldsymbol{L}^{\mathrm{T}}\boldsymbol{\mu} \right\} dt = 0 \tag{6}$$

from which the dynamic equilibrium equations will be extracted.

Integration by parts of Equation (6) yields

$$[\delta \boldsymbol{q}^{\mathrm{T}} \boldsymbol{L}^{\mathrm{T}} \boldsymbol{\mu}]_{t_1}^{t_2} + \int_{t_1}^{t_2} \delta \boldsymbol{q}^{\mathrm{T}} \left\{ -\frac{\partial \mathcal{V}}{\partial \boldsymbol{q}} - \frac{\partial \boldsymbol{\Phi}^{\mathrm{T}}}{\partial \boldsymbol{q}} \boldsymbol{\lambda} + \frac{\partial}{\partial \boldsymbol{q}} [(\boldsymbol{L}\dot{\boldsymbol{q}})^{\mathrm{T}} \boldsymbol{\mu}] - \frac{d}{dt} (\boldsymbol{L}^{\mathrm{T}} \boldsymbol{\mu}) \right\} dt = 0. \tag{7}$$

The combination of Equations (5) and (3) gives

$$\boldsymbol{\mu} = \boldsymbol{M}\boldsymbol{L}(\boldsymbol{q})\dot{\boldsymbol{q}}. \tag{8}$$

Then, the equations of motion become a first-order DAE system, with variables $\boldsymbol{q}$, $\boldsymbol{\mu}$, and $\boldsymbol{\lambda}$:

$$\begin{aligned} \boldsymbol{L}^{\mathrm{T}} \dot{\boldsymbol{\mu}} + \frac{\partial \mathcal{V}}{\partial \boldsymbol{q}} + \boldsymbol{B}^{\mathrm{T}} \boldsymbol{\lambda} + \dot{\boldsymbol{L}}^{\mathrm{T}} \boldsymbol{\mu} - \frac{\partial}{\partial \boldsymbol{q}} [(\boldsymbol{L}\dot{\boldsymbol{q}})^{\mathrm{T}} \boldsymbol{\mu}] &= \boldsymbol{0} \\ \boldsymbol{\mu} - \boldsymbol{M}\boldsymbol{L}(\boldsymbol{q})\dot{\boldsymbol{q}} &= \boldsymbol{0} \\ \boldsymbol{\Phi}(\boldsymbol{q}) &= \boldsymbol{0}, \end{aligned} \tag{9}$$

where $\boldsymbol{B} = \partial \boldsymbol{\Phi} / \partial \boldsymbol{q}$ is the Jacobian matrix of constraints. Note that the latter two terms in Equation (9a) can be written as

$$\dot{\boldsymbol{L}}^{\mathrm{T}} \boldsymbol{\mu} - \frac{\partial}{\partial \boldsymbol{q}} [(\boldsymbol{L}\dot{\boldsymbol{q}})^{\mathrm{T}} \boldsymbol{\mu}] = \boldsymbol{G}(\boldsymbol{\mu})\dot{\boldsymbol{q}}, \tag{10}$$

where the matrix $\boldsymbol{G}(\boldsymbol{\mu})$ has the following components:

$$G_{jp} = \sum_i \mu_i \left(\frac{\partial L_{ij}}{\partial q_p} - \frac{\partial L_{ip}}{\partial q_j} \right). \tag{11}$$

Skew-symmetry of $\boldsymbol{G}$ follows immediately. The final form of the equations of motion is thus:

$$\begin{aligned} \boldsymbol{L}^{\mathrm{T}} \dot{\boldsymbol{\mu}} + \frac{\partial \mathcal{V}}{\partial \boldsymbol{q}} + \boldsymbol{B}^{\mathrm{T}} \boldsymbol{\lambda} + \boldsymbol{G}(\boldsymbol{\mu})\dot{\boldsymbol{q}} &= \boldsymbol{0} \\ \boldsymbol{\mu} - \boldsymbol{M}\boldsymbol{L}(\boldsymbol{q})\dot{\boldsymbol{q}} &= \boldsymbol{0} \\ \boldsymbol{\Phi}(\boldsymbol{q}) &= \boldsymbol{0}. \end{aligned} \tag{12}$$

3 Test examples

Four test examples were chosen in order to show the performance of the different algorithms in the nonlinear regime, also taking into account the presence of nonlinear constraints and the stiff character of the differential equation. These examples are:

(a) *Nonlinear, unconstrained, nonstiff problem:* a simple pendulum with one degree of freedom $q = \theta$ (Figure 1). The expressions of kinetic and potential energies are written as:

$$\mathcal{K} = \frac{1}{2} m \dot{\theta}^2 \ell^2 \quad \mathcal{V} = (1 - \cos\theta) m g \ell$$

$m = 1$, $\ell = 1$ with $q_0 = \pi/2$ and $v_0 = 0$ are adopted as initial conditions.

Fig. 1 The simple pendulum

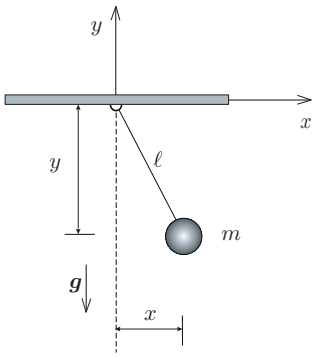

(b) *Nonlinear, constrained, nonstiff problem:* a simple pendulum modeled with two degrees of freedom $\boldsymbol{q}^{\mathrm{T}} = [x \;\; y]$ and one nonlinear constraint $\boldsymbol{\Phi} = x^2 + y^2 - \ell^2 = 0$. The expressions of the corresponding kinetic and potential energies are:

$$\mathcal{K} = \frac{1}{2} m(\dot{x}^2 + \dot{y}^2) \quad \mathcal{V} = -mgy,$$

where $m = 1$ and $\ell = 1$. Initial conditions are $\boldsymbol{x}_0^{\mathrm{T}} = [1 \;\; 0]$ and $\boldsymbol{v}_0^{\mathrm{T}} = [0 \;\; 0]$.

(c) *Nonlinear, constrained nonstiff problem:* a double pendulum modeled with four degrees of freedom and nonlinear constraints (Figure 2):

$$\boldsymbol{q}^{\mathrm{T}} = [x_1 \quad y_1 \quad x_2 \quad y_2] \quad \boldsymbol{\Phi} = \begin{bmatrix} x_1^2 + y_1^2 - \ell_1^2 \\ (x_2 - x_1)^2 + (y_2 - y_1)^2 - \ell_2^2 \end{bmatrix}.$$

The corresponding kinetic and potential energies expressions are

$$\mathcal{K} = \frac{1}{2} m_1 \left(\dot{x_1}^2 + \dot{y_1}^2\right) + \frac{1}{2} m_2 \left(\dot{x_2}^2 + \dot{y_2}^2\right) \quad \mathcal{V} = m_1 g y_1 + m_2 g y_2,$$

where $m_1 = m_2 = 1$ and $\ell_1 = \ell_2 = 1$ are adopted, with $\boldsymbol{x}_0^{\mathrm{T}} = [1\ 0\ 1\ 1]$ and $\boldsymbol{v}_0 = [0 \;\; 0 \;\; 0 \;\; 0]$ as initial conditions.

Fig. 2 The double pendulum

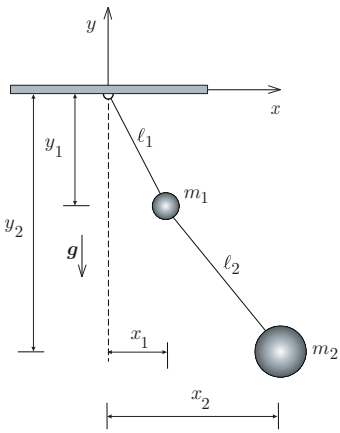

(d) *Nonlinear, constrained, stiff problem:* the same double pendulum of the previous item with a mass m_1 200 times smaller than m_2, producing in this way an ill-conditioned mass matrix: $m_1 = 0.005$ and $m_2 = 1$ are adopted.

4 The time-continuous Galerkin approximation: Energy preserving scheme

4.1 Discretization of the equation of motion

In the Galerkin approximation, the equations of motion are enforced in a weak (integral) manner. The Galerkin approximation of the equations of motion (12) is written as

$$\begin{aligned}&\frac{h}{2}\int_{-1}^{1}\mathcal{W}_1(\tau)(\dot{\boldsymbol{q}}-\boldsymbol{L}^{-1}\boldsymbol{v})d\tau\\&+\frac{h}{2}\int_{-1}^{1}\mathcal{W}_2(\tau)\left(\boldsymbol{M}\dot{\boldsymbol{v}}+\boldsymbol{L}^{-T}\boldsymbol{G}\dot{\boldsymbol{q}}+\boldsymbol{L}^{-T}\frac{\partial\mathcal{V}}{\partial\boldsymbol{q}}+\boldsymbol{L}^{-T}\boldsymbol{B}^{T}\boldsymbol{\lambda}\right)d\tau=\boldsymbol{0},\end{aligned}\tag{13}$$

where $\mathcal{W}_i(\tau)$ are the weight functions, h is the time-step size, and τ is a nondimensional time variable ($\tau=-1$ at t_n and $\tau=1$ at t_{n+1}). By using piecewise linear interpolation functions for the displacements and velocities (Figure 3) and piecewise constant test functions $\mathcal{W}_1$ and $\mathcal{W}_2$, the set of discrete equations are obtained as:

$$\begin{cases}\dfrac{1}{h}\boldsymbol{L}^{\mathrm{T}}_{n+\frac{1}{2}}\boldsymbol{M}(\boldsymbol{v}_{n+1}-\boldsymbol{v}_n)+\dfrac{1}{h}\boldsymbol{G}_{n+\frac{1}{2}}(\boldsymbol{q}_{n+1}-\boldsymbol{q}_n)+\left.\dfrac{\partial\mathcal{V}}{\partial\boldsymbol{q}}\right|_{n+\frac{1}{2}}+\boldsymbol{B}^{T}_{n+\frac{1}{2}}\boldsymbol{\lambda}_{n+\frac{1}{2}}=\boldsymbol{0}\\[2ex]\dfrac{1}{h}\boldsymbol{L}_{n+\frac{1}{2}}(\boldsymbol{q}_{n+1}-\boldsymbol{q}_n)=\dfrac{1}{2}(\boldsymbol{v}_{n+1}+\boldsymbol{v}_n)\\[2ex]\boldsymbol{\Phi}_{n+1}=\boldsymbol{0}.\end{cases}\tag{14}$$

The matrix $\boldsymbol{L}_{n+\frac{1}{2}}$ will depend on the adopted rotation parametrization. The parametrization used (Euler parameters) assures a constant matrix $\boldsymbol{L}_{n+\frac{1}{2}}$ as is shown in a previous work [20].

4.2 Energy preservation in the discrete scheme

The total energy of the system is $\mathcal{E}(\boldsymbol{q},\dot{\boldsymbol{q}})=\mathcal{K}(\dot{\boldsymbol{q}})+\mathcal{V}(\boldsymbol{q})$, where the kinetic energy has as a final expression $\mathcal{K}=\frac{1}{2}\boldsymbol{v}^{\mathrm{T}}\boldsymbol{M}\boldsymbol{v}$ and the potential energy $\mathcal{V}(\boldsymbol{q})$ is a function of the generalized coordinates $\boldsymbol{q}$. The total energy change in a time step can be evaluated computing the work done by the elastic, constraint, and inertia forces.

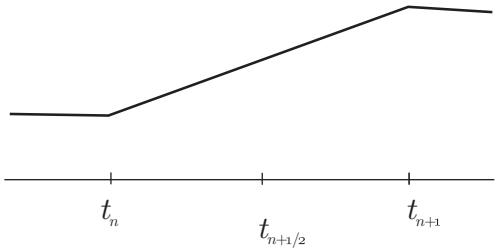

Fig. 3 The time-continuous Galerkin approximation of displacements and velocities

To prove the total energy preservation of the discrete scheme, Equation (14a) is multiplied by the displacements jump $(\boldsymbol{q}_{n+1} - \boldsymbol{q}_n)^{\mathrm{T}}$ over a time step

$$\frac{1}{h}(\boldsymbol{q}_{n+1} - \boldsymbol{q}_n)^{\mathrm{T}} \boldsymbol{L}_{n+\frac{1}{2}} \boldsymbol{M}(\boldsymbol{v}_{n+1} - \boldsymbol{v}_n) + \frac{1}{h}(\boldsymbol{q}_{n+1} - \boldsymbol{q}_n)^{\mathrm{T}} \boldsymbol{G}_{n+\frac{1}{2}}(\boldsymbol{q}_{n+1} - \boldsymbol{q}_n)$$
$$+ (\boldsymbol{q}_{n+1} - \boldsymbol{q}_n)^{\mathrm{T}} \left.\frac{\partial \mathcal{V}}{\partial \boldsymbol{q}}\right|_{n+\frac{1}{2}} + (\boldsymbol{q}_{n+1} - \boldsymbol{q}_n)^{\mathrm{T}} \boldsymbol{B}^{T}_{n+\frac{1}{2}} \boldsymbol{\lambda}_{n+\frac{1}{2}} = 0. \tag{15}$$

By looking at the first term, it can be identified that the kinetic energy jump over a time step is:

$$\frac{1}{h}(\boldsymbol{q}_{n+1} - \boldsymbol{q}_n)^{\mathrm{T}} \boldsymbol{L}_{n+\frac{1}{2}} \boldsymbol{M}(\boldsymbol{v}_{n+1} - \boldsymbol{v}_n) = \frac{1}{2}(\boldsymbol{v}_{n+1} + \boldsymbol{v}_n)^{\mathrm{T}} \boldsymbol{M}(\boldsymbol{v}_{n+1} - \boldsymbol{v}_n) = \mathcal{K}_{n+1} - \mathcal{K}_n. \tag{16}$$

Due to the skew-symmetry of the matrix $\boldsymbol{G}$, the second term becomes identically null

$$\frac{1}{h}(\boldsymbol{q}_{n+1} - \boldsymbol{q}_n)^{\mathrm{T}} \boldsymbol{G}_{n+\frac{1}{2}}(\boldsymbol{q}_{n+1} - \boldsymbol{q}_n) = \boldsymbol{0}. \tag{17}$$

In terms of elastic forces derived from the potential $\mathcal{V}$, the derivative at the midpoint $(\partial \mathcal{V}/\partial \boldsymbol{q})_{n+\frac{1}{2}}$ is substituted by the approximation $(\partial \mathcal{V}/\partial \boldsymbol{q})^{*}_{n+\frac{1}{2}}$ (*discrete directional derivative* [28]) that satisfies the next condition:

$$(\boldsymbol{q}_{n+1} - \boldsymbol{q}_n)^{\mathrm{T}} \left.\frac{\partial \mathcal{V}}{\partial \boldsymbol{q}}\right|^{*}_{n+\frac{1}{2}} = \mathcal{V}_{n+1} - \mathcal{V}_n. \tag{18}$$

In the constraint forces term, the concept of *discrete directional derivative* is used one more time, where now the Jacobian matrix of constraints $\boldsymbol{B}_{n+\frac{1}{2}}$ is replaced by the approximation $\boldsymbol{B}^{*}_{n+\frac{1}{2}}$ in order to satisfy

$$(\boldsymbol{\Phi}_{n+1} - \boldsymbol{\Phi}_n) = \boldsymbol{B}^{*}_{n+\frac{1}{2}}(\boldsymbol{q}_{n+1} - \boldsymbol{q}_n). \tag{19}$$

With this condition,

$$(\boldsymbol{q}_{n+1} - \boldsymbol{q}_n)^{\mathrm{T}} \boldsymbol{B}^{*T}_{n+\frac{1}{2}} \boldsymbol{\lambda}_{n+\frac{1}{2}} = (\boldsymbol{\Phi}_{n+1} - \boldsymbol{\Phi}_n)\, \boldsymbol{\lambda}_{n+\frac{1}{2}}. \tag{20}$$

The configuration at time t_n is assumed to be compatible, $\boldsymbol{\Phi}_n = \boldsymbol{0}$. Then, forcing

$$\boldsymbol{\Phi}_{n+1} = \boldsymbol{0} \tag{21}$$

guarantees that the work of the constraints forces is zero.

By substituting Equations (16)–(19) into Equation (15) it can be seen that the total energy change of the system over a time step results in

$$\mathcal{E}_{n+1} - \mathcal{E}_n = \mathcal{K}_{n+1} - \mathcal{K}_n + \mathcal{V}_{n+1} - \mathcal{V}_n = 0. \tag{22}$$

Therefore, the scheme formed by the equation set (14) preserves the total energy of the system if Equations (18), (19), and (21) are satisfied.

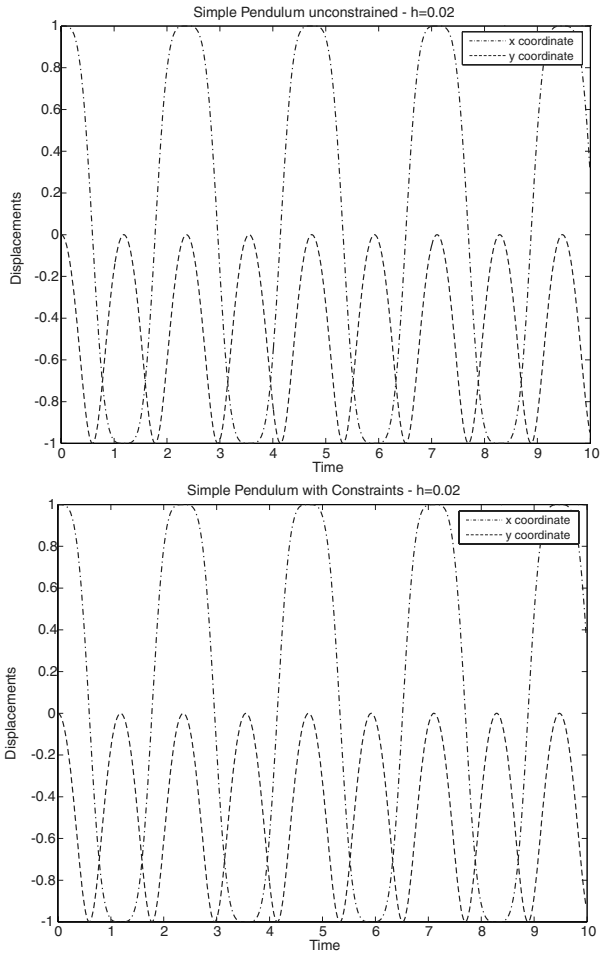

Fig. 4 Simple pendulum: displacement responses for test cases *a* and *b* in Cartesian coordinates (energy-preserving integration scheme)

4.3 Numerical examples

The energy-preserving scheme was applied to solve the four test cases. It can be observed in Figures 4 and 5 that the displacements and velocities responses computed by this scheme are correct in the first two test cases *a* and *b*, with an exact conservation of the total energy of the system (Figure 6). The nonstiff double pendulum (test case *c*) is also correctly solved (Figure 7). Finally, for the stiff double pendulum (test case *d*), although energy is exactly preserved, the ill-conditioned mass matrix generates large spurious oscillations in the numerical response which mask the response (Figure 8).

4.4 Discussion

In this section, a time integration scheme based on time-continuous Galerkin approximation with independent interpolation of displacements and velocities was introduced. A

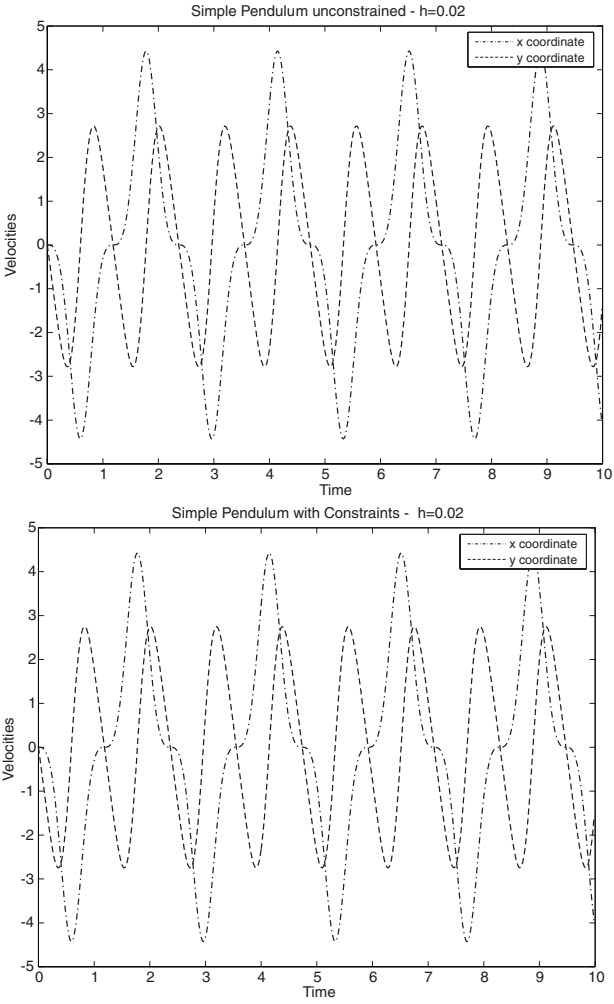

Fig. 5 Simple pendulum: velocity responses for test cases *a* and *b* in Cartesian coordinates (energy-preserving integration scheme)

discretization process was developed for elastic and inertial forces that preserves the total mechanical energy of the system at the discrete solution level. The discretized constraint forces guarantee the exact satisfaction of nonlinear constraints and the vanishing of their work over the time step. The energy-preserving scheme provides unconditional stability for nonlinear multibody systems. However, it lacks the high-frequency numerical dissipation required to tackle realistic engineering problems.

5 Time-discontinuous Galerkin approximation

In order to annihilate the spurious high-frequency oscillations that arise in flexible problems or in rigid problems with ill-conditioned mass, a new scheme that provides bounds on the

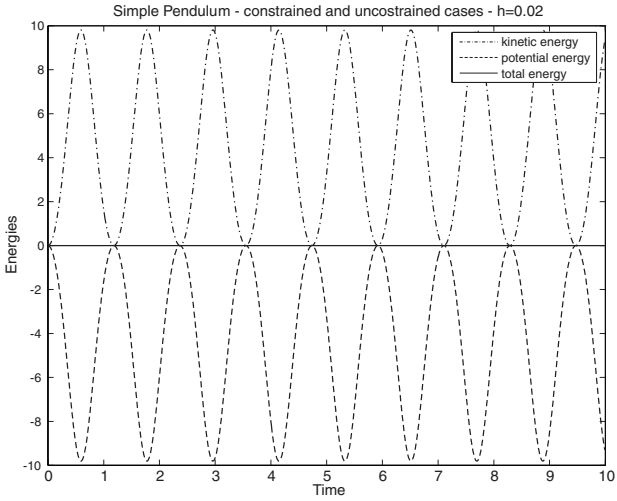

Fig. 6 Simple pendulum: kinetic, potential, and total energy for both test cases *a* and *b* (energy-preserving integration scheme). Note that curves for both test cases are superposed

algorithmic total energy over a typical time step $[t_n, t_{n+1}]$ and at the same time introduces dissipation in the high-frequency regime will be constructed. For this purpose, the time-discontinuous Galerkin approximation will be used, which is a natural way to arrive at the set of discrete equations of an algorithmic total energy dissipative scheme [21].

Discontinuities on displacements and velocity fields $\boldsymbol{q}$ and $\boldsymbol{v}$ at the initial time t_n are allowed in this scheme (Figure 9). A contribution taking into account the value of these discontinuities will appear in the weighted residual expressions. An additional state at time $t_j = \lim_{\varepsilon \to 0}(t_n + \varepsilon)$ is added and the following averaged quantities at the middle points are defined:

$$(\cdot)_g = \frac{1}{2}((\cdot)_{n+1} + (\cdot)_j), \quad (\cdot)_h = \frac{1}{2}((\cdot)_j + (\cdot)_n). \tag{23}$$

The scheme moves forward from the initial to the final time through two coupled steps, one from t_n to t_j and the other from t_j to t_{n+1}.

5.1 Energy decaying scheme without control of the amount of the dissipated energy

5.1.1 Discretization of the equation of motion

The discontinuous Galerkin approximation of the equations of motion (12) can be written as:

$$\begin{aligned}
&\frac{h}{2}\int_{-1}^{1} \mathcal{W}_1(\tau)[\dot{\boldsymbol{q}} - \boldsymbol{L}^{-1}\boldsymbol{v}]d\tau \\
&\quad + \frac{h}{2}\int_{-1}^{1} \mathcal{W}_2(\tau)\left[\boldsymbol{M}\dot{\boldsymbol{v}} + \boldsymbol{L}^{-\mathrm{T}}\boldsymbol{G}\dot{\boldsymbol{q}} + \boldsymbol{L}^{-\mathrm{T}}\frac{\partial \mathcal{V}}{\partial \boldsymbol{q}} + \boldsymbol{L}^{-\mathrm{T}}\boldsymbol{B}^{\mathrm{T}}\boldsymbol{\lambda}\right]d\tau \\
&\quad + \mathcal{W}_1(-1)(\boldsymbol{q}_j - \boldsymbol{q}_n) + \mathcal{W}_2(-1)[\boldsymbol{M}(\boldsymbol{v}_j - \boldsymbol{v}_n) + \boldsymbol{L}^{-\mathrm{T}}\boldsymbol{G}_h(\boldsymbol{q}_j - \boldsymbol{q}_n)] = \boldsymbol{0},
\end{aligned} \tag{24}$$

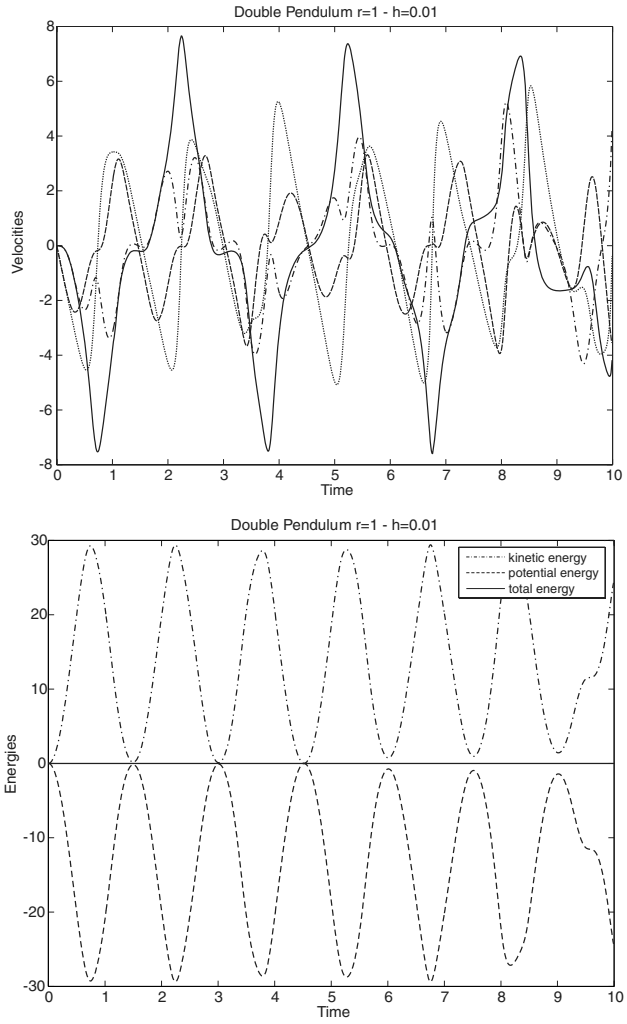

Fig. 7 Double pendulum: time responses for velocities and energies in Cartesian coordinates for $m_1 = m_2 = 1$, for test case *c* (energy-preserving integration scheme)

where the test functions are

$$\mathcal{W}_1(\tau) = A_1 + B_1\tau, \quad \mathcal{W}_2(\tau) = A_2 + B_2\tau. \tag{25}$$

Displacements and velocities are linearly interpolated over the time step $[t_j, t_{n+1}]$:

$$\begin{aligned} \boldsymbol{q} &= \frac{\boldsymbol{q}_j(1-\tau) + \boldsymbol{q}_{n+1}(1+\tau)}{2}, \quad \dot{\boldsymbol{q}} = \frac{(\boldsymbol{q}_{n+1} - \boldsymbol{q}_j)}{h} \\ \boldsymbol{v} &= \frac{\boldsymbol{v}_j(1-\tau) + \boldsymbol{v}_{n+1}(1+\tau)}{2}, \quad \dot{\boldsymbol{v}} = \frac{(\boldsymbol{v}_{n+1} - \boldsymbol{v}_j)}{h}. \end{aligned} \tag{26}$$

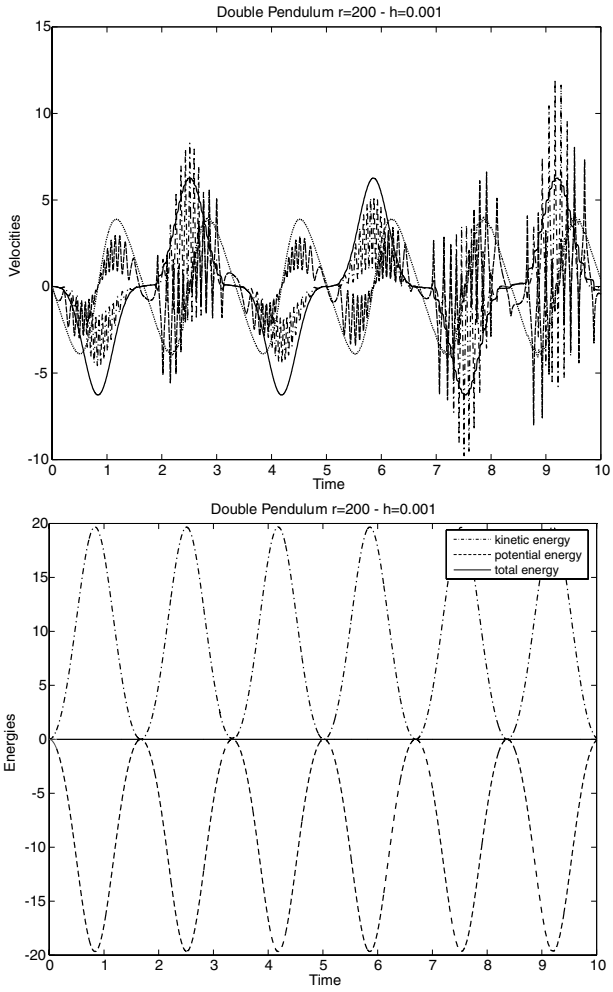

Fig. 8 Double pendulum: time responses for velocities and energies in Cartesian coordinates for $m_1 = 0.005$ and $m_2 = 1$ for test case d (energy-preserving integration scheme)

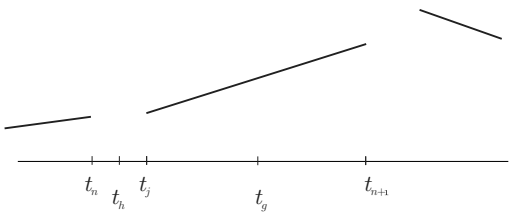

Fig. 9 Discontinuous Galerkin approximation of displacements and velocities

Internal and constraint forces are similarly interpolated, by grouping the contributions at the midpoint g:

$$\begin{aligned} \frac{\partial \mathcal{V}}{\partial \boldsymbol{q}} &= \left.\frac{\partial \mathcal{V}}{\partial \boldsymbol{q}}\right|_g + \frac{\tau}{2}\left(\left.\frac{\partial \mathcal{V}}{\partial \boldsymbol{q}}\right|_{n+1} - \left.\frac{\partial \mathcal{V}}{\partial \boldsymbol{q}}\right|_j\right) \\ \boldsymbol{B}^{\mathrm{T}}\boldsymbol{\lambda} &= \boldsymbol{B}_g^{\mathrm{T}}\boldsymbol{\lambda}_g + \frac{\tau}{2}\left[\boldsymbol{B}_{n+1}^{\mathrm{T}}\boldsymbol{\lambda}_{n+1} - \boldsymbol{B}_j^{\mathrm{T}}\boldsymbol{\lambda}_j\right]. \end{aligned} \tag{27}$$

By taking independent variations on the parameters A_1, A_2, B_1, and B_2, the following discrete equations system is obtained, which is solved in an iterative form to obtain $\boldsymbol{q}_{n+1}$, $\boldsymbol{q}_j$, $\boldsymbol{v}_{n+1}$, $\boldsymbol{v}_j$, $\boldsymbol{\lambda}_g$, and $\boldsymbol{\lambda}_j$

$$\begin{cases} \dfrac{1}{h}\boldsymbol{L}^{\mathrm{T}}\boldsymbol{M}\left(\boldsymbol{v}_{n+1}-\boldsymbol{v}_n\right) + \left.\dfrac{\partial \mathcal{V}}{\partial \boldsymbol{q}}\right|_g + \boldsymbol{B}_g^{\mathrm{T}}\boldsymbol{\lambda}_g + \dfrac{1}{h}\boldsymbol{G}_m(\boldsymbol{q}_{n+1}-\boldsymbol{q}_n) = \boldsymbol{0} \\ \dfrac{1}{h}\boldsymbol{L}^{\mathrm{T}}\boldsymbol{M}\left(\boldsymbol{v}_j-\boldsymbol{v}_n\right) - \dfrac{1}{3}\left[\left.\dfrac{\partial \mathcal{V}}{\partial \boldsymbol{q}}\right|_g - \left.\dfrac{\partial \mathcal{V}}{\partial \boldsymbol{q}}\right|_h\right] + \dfrac{1}{6}\left[\left.\dfrac{\partial \mathcal{V}}{\partial \boldsymbol{q}}\right|_j - \left.\dfrac{\partial \mathcal{V}}{\partial \boldsymbol{q}}\right|_n\right] \\ \quad - \dfrac{1}{3}\left(\boldsymbol{B}_g^{T}\boldsymbol{\lambda}_g - \boldsymbol{B}_h^{T}\boldsymbol{\lambda}_j\right) + \dfrac{1}{h}\boldsymbol{G}_h(\boldsymbol{q}_j-\boldsymbol{q}_n) = \boldsymbol{0} \\ \dfrac{1}{h}\boldsymbol{L}(\boldsymbol{q}_{n+1}-\boldsymbol{q}_n) - \dfrac{1}{2}(\boldsymbol{v}_{n+1}-\boldsymbol{v}_j) = \boldsymbol{0} \\ \dfrac{1}{h}\boldsymbol{L}(\boldsymbol{q}_j-\boldsymbol{q}_n) + \dfrac{1}{6}(\boldsymbol{v}_{n+1}-\boldsymbol{v}_j) = \boldsymbol{0} \\ \boldsymbol{\Phi}_j = \boldsymbol{0} \\ \boldsymbol{\Phi}_{n+1} = \boldsymbol{0}. \end{cases} \tag{28}$$

The fact that $\boldsymbol{L}$ is constant for the adopted rotation parametrization and the following approximation have been used:

$$\boldsymbol{G}_g(\boldsymbol{q}_{n+1}-\boldsymbol{q}_j) + \boldsymbol{G}_h(\boldsymbol{q}_j-\boldsymbol{q}_n) \simeq \boldsymbol{G}_m(\boldsymbol{q}_{n+1}-\boldsymbol{q}_n) \tag{29}$$

with:

$$\boldsymbol{G}_m = \boldsymbol{G}_m(\boldsymbol{H}_m); \quad \boldsymbol{H}_m = \frac{1}{2}(\boldsymbol{H}_n + \boldsymbol{H}_{n+1}) = \frac{1}{2}\boldsymbol{J}(\boldsymbol{\Omega}_n + \boldsymbol{\Omega}_{n+1}) \tag{30}$$

5.1.2 Energy decay in the discrete scheme

If Equation (28a) is multiplied by the displacements jump $(\boldsymbol{q}_{n+1}-\boldsymbol{q}_n)$ and Equation (28b) by $(\boldsymbol{q}_j-\boldsymbol{q}_n)$, we can get:

$$\begin{aligned} &\frac{1}{h}(\boldsymbol{q}_{n+1}-\boldsymbol{q}_n)^{\mathrm{T}}\boldsymbol{L}^{\mathrm{T}}\boldsymbol{M}(\boldsymbol{v}_{n+1}-\boldsymbol{v}_n) + (\boldsymbol{q}_{n+1}-\boldsymbol{q}_n)^{\mathrm{T}}\left.\frac{\partial \mathcal{V}}{\partial \boldsymbol{q}}\right|_g \\ &\quad + (\boldsymbol{q}_{n+1}-\boldsymbol{q}_n)^{\mathrm{T}}\boldsymbol{B}_g^{T}\boldsymbol{\lambda}_g + \frac{1}{h}(\boldsymbol{q}_{n+1}-\boldsymbol{q}_n)^{\mathrm{T}}\boldsymbol{G}_m(\boldsymbol{q}_{n+1}-\boldsymbol{q}_n) = 0 \end{aligned}$$

$$\frac{1}{h}(\boldsymbol{q}_j-\boldsymbol{q}_n)^{\mathrm{T}}\boldsymbol{L}^{\mathrm{T}}\boldsymbol{M}(\boldsymbol{v}_j-\boldsymbol{v}_n)-\frac{1}{3}(\boldsymbol{q}_j-\boldsymbol{q}_n)^{\mathrm{T}}\left[\left.\frac{\partial\mathcal{V}}{\partial\boldsymbol{q}}\right|_g-\left.\frac{\partial\mathcal{V}}{\partial\boldsymbol{q}}\right|_h\right]$$
$$+\frac{1}{6}(\boldsymbol{q}_j-\boldsymbol{q}_n)^{\mathrm{T}}\left[\left.\frac{\partial\mathcal{V}}{\partial\boldsymbol{q}}\right|_j-\left.\frac{\partial\mathcal{V}}{\partial\boldsymbol{q}}\right|_n\right]-\frac{1}{3}(\boldsymbol{q}_j-\boldsymbol{q}_n)^{\mathrm{T}}\left(\boldsymbol{B}_g^T\boldsymbol{\lambda}_g-\boldsymbol{B}_h^T\boldsymbol{\lambda}_j\right)$$
$$+\frac{1}{h}(\boldsymbol{q}_j-\boldsymbol{q}_n)^{\mathrm{T}}\boldsymbol{G}_h(\boldsymbol{q}_j-\boldsymbol{q}_n)=0. \tag{31}$$

By using the displacements–velocities relationships (28c) and (28d) and by linearly combining Equations (31a) and (31b):

$$\frac{1}{2}(\boldsymbol{v}_{n+1}+\boldsymbol{v}_j)^{\mathrm{T}}\boldsymbol{M}(\boldsymbol{v}_{n+1}-\boldsymbol{v}_n)-\frac{1}{2}(\boldsymbol{v}_{n+1}-\boldsymbol{v}_j)^{\mathrm{T}}\boldsymbol{M}(\boldsymbol{v}_j-\boldsymbol{v}_n)$$
$$+(\boldsymbol{q}_{n+1}-\boldsymbol{q}_j)^{\mathrm{T}}\left.\frac{\partial\mathcal{V}}{\partial\boldsymbol{q}}\right|_g+(\boldsymbol{q}_j-\boldsymbol{q}_n)^{\mathrm{T}}\left.\frac{\partial\mathcal{V}}{\partial\boldsymbol{q}}\right|_h+\frac{1}{2}(\boldsymbol{q}_j-\boldsymbol{q}_n)^{\mathrm{T}}\left[\left.\frac{\partial\mathcal{V}}{\partial\boldsymbol{q}}\right|_j-\left.\frac{\partial\mathcal{V}}{\partial\boldsymbol{q}}\right|_n\right]$$
$$+(\boldsymbol{q}_{n+1}-\boldsymbol{q}_n)^{\mathrm{T}}\boldsymbol{B}_g^T\boldsymbol{\lambda}_g-(\boldsymbol{q}_j-\boldsymbol{q}_n)^{\mathrm{T}}\left(\boldsymbol{B}_g^T\boldsymbol{\lambda}_g-\boldsymbol{B}_h^T\boldsymbol{\lambda}_j\right)$$
$$+(\boldsymbol{q}_{n+1}-\boldsymbol{q}_n)^{\mathrm{T}}\frac{1}{h}\boldsymbol{G}_m(\boldsymbol{q}_{n+1}-\boldsymbol{q}_n)+(\boldsymbol{q}_j-\boldsymbol{q}_n)^{\mathrm{T}}\frac{1}{h}\boldsymbol{G}_h(\boldsymbol{q}_j-\boldsymbol{q}_n)=\boldsymbol{0}. \tag{32}$$

After some algebraic manipulations, it can be shown that the first two terms are equal to the sum of the kinetic energy jump over the time step $[t_n, t_{n+1}]$ plus a positive term $\mathcal{K}_{nj}$ which can be called *kinetic energy of the jump*:

$$\frac{1}{2}(\boldsymbol{v}_{n+1}+\boldsymbol{v}_n)^{\mathrm{T}}\boldsymbol{M}(\boldsymbol{v}_{n+1}-\boldsymbol{v}_j)-\frac{1}{2}(\boldsymbol{v}_{n+1}-\boldsymbol{v}_j)^{\mathrm{T}}\boldsymbol{M}(\boldsymbol{v}_j-\boldsymbol{v}_n)=\mathcal{K}_{n+1}-\mathcal{K}_n+\mathcal{K}_{nj}, \tag{33}$$

where the *kinetic energy of the jump* is defined as

$$\mathcal{K}_{nj}=\frac{1}{2}(\boldsymbol{v}_j-\boldsymbol{v}_n)^{\mathrm{T}}\boldsymbol{M}(\boldsymbol{v}_j-\boldsymbol{v}_n)\geqq 0. \tag{34}$$

Once again, the midpoint elastic forces $(\partial\mathcal{V}/\partial\boldsymbol{q})_g$ and $(\partial\mathcal{V}/\partial\boldsymbol{q})_h$ are replaced by their *discrete directional derivative* counterparts, giving the jump of potential energy over the time step:

$$(\boldsymbol{q}_{n+1}-\boldsymbol{q}_j)^{\mathrm{T}}\left.\frac{\partial\mathcal{V}}{\partial\boldsymbol{q}}\right|_g^*+(\boldsymbol{q}_j-\boldsymbol{q}_n)^{\mathrm{T}}\left.\frac{\partial\mathcal{V}}{\partial\boldsymbol{q}}\right|_h^*=\mathcal{V}_{n+1}-\mathcal{V}_j+\mathcal{V}_j-\mathcal{V}_n=\mathcal{V}_{n+1}-\mathcal{V}_n. \tag{35}$$

The third term in Equation (32) involving derivatives of potential energy will be called *potential energy of the jump*; it is nonnegative for convex potential energy functions:

$$\mathcal{V}_{nj}=\frac{1}{2}(\boldsymbol{q}_j-\boldsymbol{q}_n)^{\mathrm{T}}\left[\left.\frac{\partial\mathcal{V}}{\partial\boldsymbol{q}}\right|_j-\left.\frac{\partial\mathcal{V}}{\partial\boldsymbol{q}}\right|_n\right]\geqq 0. \tag{36}$$

For the constraint forces, the matrices $\boldsymbol{B}_g$ and $\boldsymbol{B}_h$ are approximated with $\boldsymbol{B}_g^*$ and $\boldsymbol{B}_h^*$, using once again the concept of *discrete directional derivative* in such a way that

$$\boldsymbol{B}_g^*(\boldsymbol{q}_{n+1} - \boldsymbol{q}_j) = \boldsymbol{\Phi}_{n+1} - \boldsymbol{\Phi}_j; \quad \boldsymbol{B}_h^*(\boldsymbol{q}_j - \boldsymbol{q}_n) = \boldsymbol{\Phi}_j - \boldsymbol{\Phi}_n. \tag{37}$$

Then,

$$\begin{aligned}(\boldsymbol{q}_{n+1} - \boldsymbol{q}_n)^{\mathrm{T}} \boldsymbol{B}_g^{*T} \boldsymbol{\lambda}_g - (\boldsymbol{q}_j - \boldsymbol{q}_n)^{\mathrm{T}} \left(\boldsymbol{B}_g^{*T} \boldsymbol{\lambda}_g - \boldsymbol{B}_h^{*T} \boldsymbol{\lambda}_j\right) \\ = (\boldsymbol{\Phi}_{n+1} - \boldsymbol{\Phi}_j)^{\mathrm{T}} \boldsymbol{\lambda}_g + (\boldsymbol{\Phi}_j - \boldsymbol{\Phi}_n)^{\mathrm{T}} \boldsymbol{\lambda}_j.\end{aligned} \tag{38}$$

The configuration at time t_n is assumed to be compatible, $\boldsymbol{\Phi}_n = \boldsymbol{0}$. Then, by enforcing

$$\boldsymbol{\Phi}_j = \boldsymbol{0} \quad \text{and} \quad \boldsymbol{\Phi}_{n+1} = \boldsymbol{0} \tag{39}$$

implies that the work of the constraints forces vanishes.

Finally, for the last two terms:

$$\begin{aligned}(\boldsymbol{q}_{n+1} - \boldsymbol{q}_n)^{\mathrm{T}} \frac{1}{h} \boldsymbol{G}_m (\boldsymbol{q}_{n+1} - \boldsymbol{q}_n) = 0 \\ (\boldsymbol{q}_j - \boldsymbol{q}_n)^{\mathrm{T}} \frac{1}{h} \boldsymbol{G}_h (\boldsymbol{q}_j - \boldsymbol{q}_n) = 0\end{aligned} \tag{40}$$

because of the skew-symmetry of $\boldsymbol{G}_m$ and $\boldsymbol{G}_h$.

By substituting Equations (33)–(37) and (40) in Equation (32), it can be seen that the change of the total energy of the system becomes

$$\mathcal{K}_{n+1} - \mathcal{K}_n + \mathcal{V}_{n+1} - \mathcal{V}_n + c^2 = \mathcal{E}_{n+1} - \mathcal{E}_n + c^2 = 0, \tag{41}$$

where the quadratic term is the *total energy of the jump*

$$c^2 = \mathcal{E}_{nj} = \mathcal{K}_{nj} + \mathcal{V}_{nj} \geqq 0. \tag{42}$$

Finally,

$$\mathcal{E}_{n+1} = \mathcal{E}_n - c^2 \longrightarrow \mathcal{E}_{n+1} \leqq \mathcal{E}_n, \tag{43}$$

that is, the scheme proposed by the set of Equation (28) implies the inequality (43), which guarantees the decay of the total energy of the system if Equations (35)–(37) and (39) are satisfied.

5.1.3 Numerical examples

In the test examples solved using the proposed energy decaying scheme, it can be observed that the numerical oscillations that appeared in the double pendulum with ill-conditioned mass matrix, are now completely damped out (Figure 10). However, Figure 11 shows that the scheme dissipates too much energy. For the simple pendulum, the responses are plotted in Figures 12 and 13. It can be observed that although the results of the unconstrained case are correct, in the case of the constrained model the energy dissipation is again excessive.

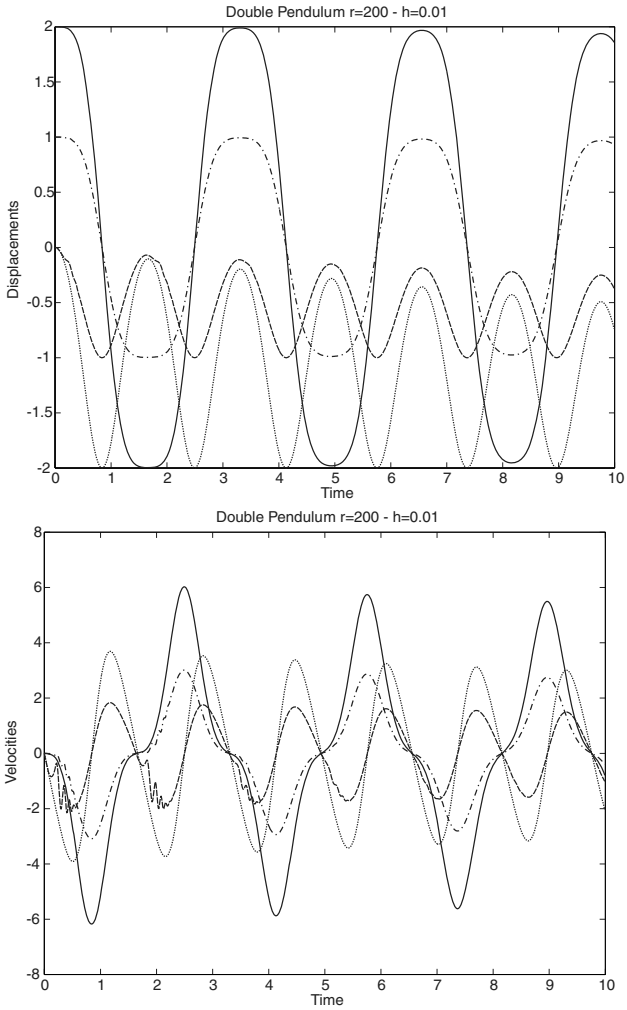

Fig. 10 Double pendulum: time responses for displacements and velocities in Cartesian coordinates for $m_1 = 0.005$, $m_2 = 1$, in test-case d (energy-decaying integration scheme without dissipation control)

5.1.4 Discussion

A time integration scheme based on time-discontinuous Galerkin approximation with independent interpolation of displacements and velocities was developed. The scheme is closely related to the energy preserving scheme and it implies a discrete energy decay statement. The discretization process for the constraint forces is left unchanged, that is, the work they perform vanishes exactly and constraints are exactly satisfied. This procedure provides nonlinear unconditional stability and high-frequency numerical dissipation. Note that there is no control on the amount of dissipated energy. Note also that, although unconstrained problems are solved correctly with a small amount of dissipation, the computed solutions for nonlinear constrained problems present an excessive amount of energy dissipation.

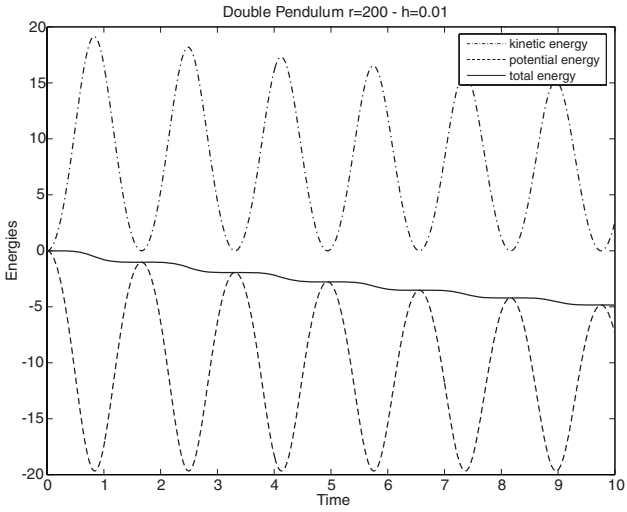

Fig. 11 Double pendulum: time responses for kinetic, potential, and total energy for $m_1 = 0.005$ and $m_2 = 1$, in test-case *d* (energy-decaying integration scheme without dissipation control)

5.2 Energy decaying scheme with control of dissipated energy

The algorithm proposed in the previous section is extended to include an algorithmic control in the amount of numerical dissipation. The procedure is exactly the same as before but the expressions of the interpolated displacements, velocities, and internal forces are now:

$$\boldsymbol{q} = \frac{(\boldsymbol{q}_j + \boldsymbol{q}_{n+1})}{2} + \tau \frac{(\boldsymbol{q}_{n+1} - \alpha \boldsymbol{q}_j - (1-\alpha)\boldsymbol{q}_n)}{2}, \quad \dot{\boldsymbol{q}} = \frac{(\boldsymbol{q}_{n+1} - \boldsymbol{q}_j)}{h}$$

$$\boldsymbol{v} = \frac{(\boldsymbol{v}_j + \boldsymbol{v}_{n+1})}{2} + \tau \frac{(\boldsymbol{v}_{n+1} - \alpha \boldsymbol{v}_j - (1-\alpha)\boldsymbol{v}_n)}{2}, \quad \dot{\boldsymbol{v}} = \frac{(\boldsymbol{v}_{n+1} - \boldsymbol{v}_j)}{h} \tag{44}$$

$$\frac{\partial \mathcal{V}}{\partial \boldsymbol{q}} = \left.\frac{\partial \mathcal{V}}{\partial \boldsymbol{q}}\right|_g + \frac{\tau}{2}\left[\left.\frac{\partial \mathcal{V}}{\partial \boldsymbol{q}}\right|_{n+1} - \alpha \left.\frac{\partial \mathcal{V}}{\partial \boldsymbol{q}}\right|_j - (1-\alpha) \left.\frac{\partial \mathcal{V}}{\partial \boldsymbol{q}}\right|_n \right], \tag{45}$$

where the algorithmic parameter $\alpha \in [0, 1]$ will be shown to control the amount of dissipation. On the contrary, the forces of constraint are interpolated as in the previous scheme:

$$\boldsymbol{B}^{\mathrm{T}}\boldsymbol{\lambda} = \boldsymbol{B}_g^{\mathrm{T}}\boldsymbol{\lambda}_g + \frac{\tau}{2}\left(\boldsymbol{B}_{n+1}^{\mathrm{T}}\boldsymbol{\lambda}_{n+1} - \boldsymbol{B}_j^{\mathrm{T}}\boldsymbol{\lambda}_j\right). \tag{46}$$

The weight functions are the same used for the previous scheme.

5.2.1 Discretization of the equation of motion

A weighted residual expression of the equations of motion (12) is formed, as in the previous scheme, and after integration, the TDG discrete form of the equations of motion can be

written as:

$$\begin{cases} \dfrac{1}{h}\boldsymbol{L}^{\mathrm{T}}\boldsymbol{M}(\boldsymbol{v}_{n+1}-\boldsymbol{v}_n)+\dfrac{1}{h}\boldsymbol{G}_m(\boldsymbol{q}_{n+1}-\boldsymbol{q}_n)+\left.\dfrac{\partial\mathcal{V}}{\partial\boldsymbol{q}}\right|_g+(\boldsymbol{B}^{\mathrm{T}}\boldsymbol{\lambda})_g=\boldsymbol{0} \\ \dfrac{1}{h}\boldsymbol{L}^{\mathrm{T}}\boldsymbol{M}(\boldsymbol{v}_j-\boldsymbol{v}_n)+\dfrac{1}{h}\boldsymbol{G}_h(\boldsymbol{q}_j-\boldsymbol{q}_n)-\dfrac{1}{3}\left[\left.\dfrac{\partial\mathcal{V}}{\partial\boldsymbol{q}}\right|_g-\left.\dfrac{\partial\mathcal{V}}{\partial\boldsymbol{q}}\right|_h\right] \\ \quad+\dfrac{1}{6}\alpha\left[\left.\dfrac{\partial\mathcal{V}}{\partial\boldsymbol{q}}\right|_j-\left.\dfrac{\partial\mathcal{V}}{\partial\boldsymbol{q}}\right|_n\right]-\dfrac{1}{3}\left(\boldsymbol{B}_g^{\mathrm{T}}\boldsymbol{\lambda}_g-\boldsymbol{B}_h^{\mathrm{T}}\boldsymbol{\lambda}_j\right)=\boldsymbol{0} \\ \boldsymbol{L}\dfrac{1}{h}(\boldsymbol{q}_{n+1}-\boldsymbol{q}_n)=\dfrac{1}{2}(\boldsymbol{v}_j+\boldsymbol{v}_{n+1}) \\ \boldsymbol{L}\dfrac{1}{h}(\boldsymbol{q}_j-\boldsymbol{q}_n)=-\dfrac{1}{6}\left[\boldsymbol{v}_{n+1}-\alpha\boldsymbol{v}_j+(\alpha-1)\boldsymbol{v}_n\right] \\ \boldsymbol{\Phi}_j=\boldsymbol{0} \\ \boldsymbol{\Phi}_{n+1}=\boldsymbol{0} \end{cases} \tag{47}$$

with $0\leq\alpha\leq 1$.

5.2.2 Energy decay in the discrete scheme

The decay of energy for this scheme will be proved now. For this purpose, Equation (47a) is multiplied by $(\boldsymbol{q}_{n+1}-\boldsymbol{q}_n)^{\mathrm{T}}$ and Equation (47b) by $(\boldsymbol{q}_j-\boldsymbol{q}_n)^{\mathrm{T}}$ to get

$$\begin{aligned} &\frac{1}{h}(\boldsymbol{q}_{n+1}-\boldsymbol{q}_n)^{\mathrm{T}}\boldsymbol{L}^{\mathrm{T}}\boldsymbol{M}(\boldsymbol{v}_{n+1}-\boldsymbol{v}_n)+\frac{1}{h}(\boldsymbol{q}_{n+1}-\boldsymbol{q}_n)^{\mathrm{T}}\boldsymbol{G}_m(\boldsymbol{q}_{n+1}-\boldsymbol{q}_n) \\ &\quad+(\boldsymbol{q}_{n+1}-\boldsymbol{q}_n)^{\mathrm{T}}\left.\frac{\partial\mathcal{V}}{\partial\boldsymbol{q}}\right|_g+(\boldsymbol{q}_{n+1}-\boldsymbol{q}_n)^{\mathrm{T}}(\boldsymbol{B}^{\mathrm{T}}\boldsymbol{\lambda})_g=0 \end{aligned} \tag{48}$$

$$\begin{aligned} &\frac{1}{h}(\boldsymbol{q}_j-\boldsymbol{q}_n)^{\mathrm{T}}\boldsymbol{L}^{\mathrm{T}}\boldsymbol{M}(\boldsymbol{v}_j-\boldsymbol{v}_n)+\frac{1}{h}(\boldsymbol{q}_j-\boldsymbol{q}_n)^{\mathrm{T}}\boldsymbol{G}_h(\boldsymbol{q}_j-\boldsymbol{q}_n) \\ &\quad-(\boldsymbol{q}_j-\boldsymbol{q}_n)^{\mathrm{T}}\frac{1}{3}\left[\left.\frac{\partial\mathcal{V}}{\partial\boldsymbol{q}}\right|_g-\left.\frac{\partial\mathcal{V}}{\partial\boldsymbol{q}}\right|_h\right]+(\boldsymbol{q}_j-\boldsymbol{q}_n)^{\mathrm{T}}\frac{1}{6}\alpha\left[\left.\frac{\partial\mathcal{V}}{\partial\boldsymbol{q}}\right|_j-\left.\frac{\partial\mathcal{V}}{\partial\boldsymbol{q}}\right|_n\right] \\ &\quad-(\boldsymbol{q}_j-\boldsymbol{q}_n)^{\mathrm{T}}\frac{1}{3}\left(\boldsymbol{B}_g^{\mathrm{T}}\boldsymbol{\lambda}-\boldsymbol{B}_h^{\mathrm{T}}\boldsymbol{\lambda}_j\right)=0. \end{aligned} \tag{49}$$

Combining linearly the latter two expressions:

$$\begin{aligned} &\frac{1}{2}(\boldsymbol{v}_j+\boldsymbol{v}_{n+1})^{\mathrm{T}}\boldsymbol{M}(\boldsymbol{v}_{n+1}-\boldsymbol{v}_n)-\frac{1}{2}[\boldsymbol{v}_{n+1}-\alpha\boldsymbol{v}_j+(\alpha-1)\boldsymbol{v}_n]^{\mathrm{T}}\boldsymbol{M}(\boldsymbol{v}_j-\boldsymbol{v}_n) \\ &\quad+(\boldsymbol{q}_{n+1}-\boldsymbol{q}_n)^{\mathrm{T}}\left.\frac{\partial\mathcal{V}}{\partial\boldsymbol{q}}\right|_g-(\boldsymbol{q}_j-\boldsymbol{q}_n)^{\mathrm{T}}\frac{1}{2}\left[\left.\frac{\partial\mathcal{V}}{\partial\boldsymbol{q}}\right|_g-\left.\frac{\partial\mathcal{V}}{\partial\boldsymbol{q}}\right|_h\right]+ \\ &\quad-(\boldsymbol{q}_j-\boldsymbol{q}_n)^{\mathrm{T}}\frac{1}{2}\alpha\left[\left.\frac{\partial\mathcal{V}}{\partial\boldsymbol{q}}\right|_j-\left.\frac{\partial\mathcal{V}}{\partial\boldsymbol{q}}\right|_n\right] \\ &\quad+(\boldsymbol{q}_{n+1}-\boldsymbol{q}_n)^{\mathrm{T}}\boldsymbol{B}_g^{\mathrm{T}}\boldsymbol{\lambda}_g-(\boldsymbol{q}_j-\boldsymbol{q}_n)^{\mathrm{T}}\left(\boldsymbol{B}_g^{\mathrm{T}}\boldsymbol{\lambda}_g-\boldsymbol{B}_h^{\mathrm{T}}\boldsymbol{\lambda}_j\right)=0, \end{aligned} \tag{50}$$

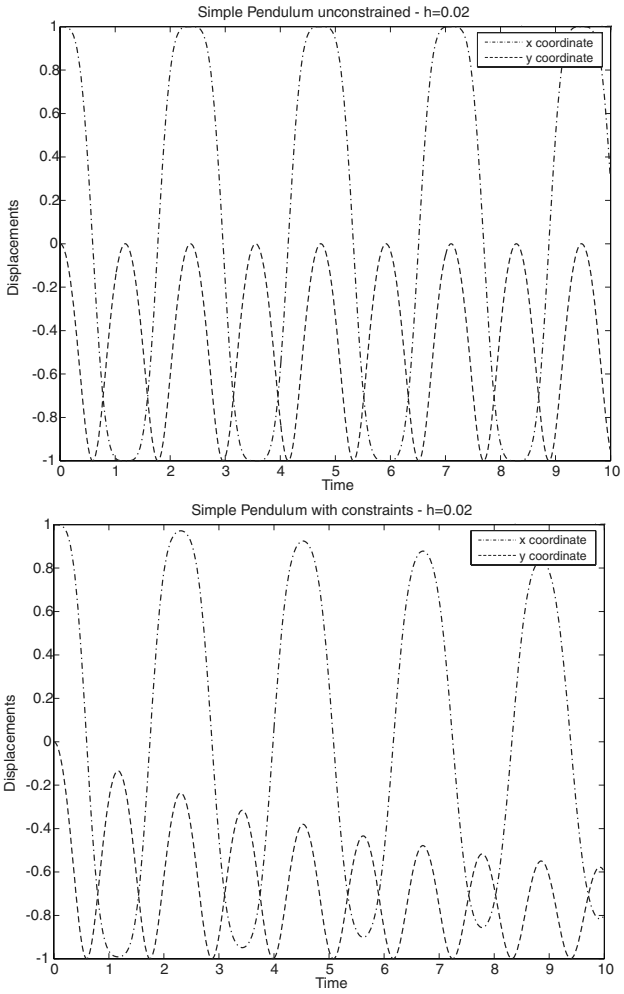

Fig. 12 Simple pendulum: displacements for test cases *a* and *b* in Cartesian coordinates (energy-decaying integration scheme without dissipation control)

where, after some algebraic manipulations, the terms corresponding to the kinetic energy jump $\mathcal{K}_{n+1} - \mathcal{K}_n$, and to the *kinetic energy of the jump* $\mathcal{K}_{nj}$, multiplied by the factor α can be identified:

$$\frac{1}{2}(\boldsymbol{v}_j + \boldsymbol{v}_{n+1})^{\mathrm{T}}\boldsymbol{M}(\boldsymbol{v}_{n+1} - \boldsymbol{v}_n) - \frac{1}{2}[\boldsymbol{v}_{n+1} - \alpha\boldsymbol{v}_j + (\alpha - 1)\boldsymbol{v}_n]^{\mathrm{T}}\boldsymbol{M}(\boldsymbol{v}_j - \boldsymbol{v}_n)$$
$$= \mathcal{K}_{n+1} - \mathcal{K}_n + \alpha\mathcal{K}_{nj} = \mathcal{K}_{n+1} - \mathcal{K}_n + \alpha\mathcal{K}_{nj}.$$

The expression of the *kinetic energy of the jump* is as before:

$$\mathcal{K}_{nj} = \frac{1}{2}(\boldsymbol{v}_j - \boldsymbol{v}_n)^{\mathrm{T}}\boldsymbol{M}(\boldsymbol{v}_j - \boldsymbol{v}_n) \geqq 0. \tag{51}$$

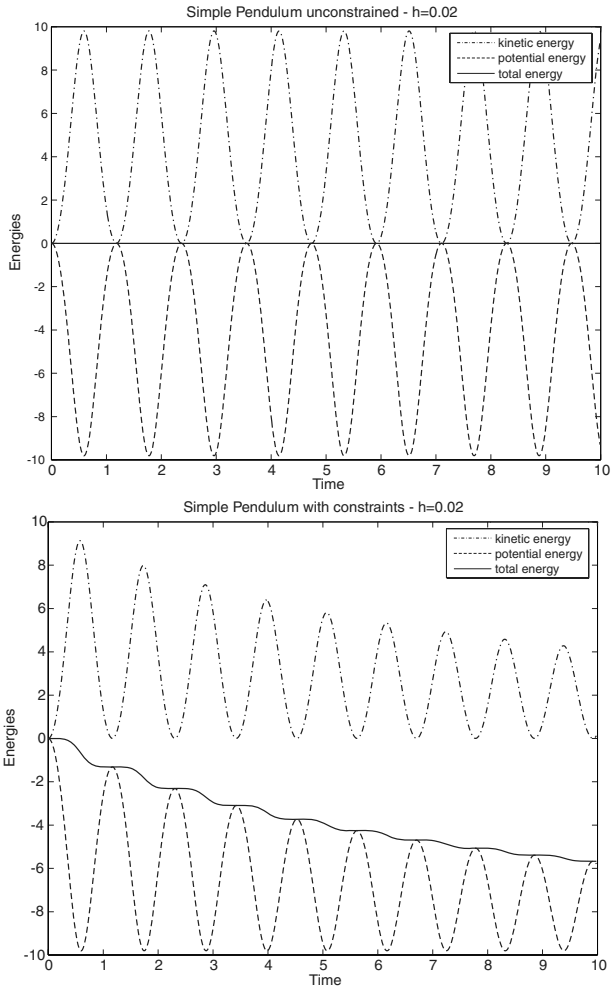

Fig. 13 Simple pendulum: kinetic, potential and total energy for test cases *a* and *b* (energy-decaying integration scheme without dissipation control)

Once again, the concept of the *discrete directional derivative* for the potential energy terms will be used, in order to replace the expressions $(\partial \mathcal{V}/\partial \boldsymbol{q})_g$ and $(\partial \mathcal{V}/\partial \boldsymbol{q})_h$ by their discrete directional counterparts in order to verify Equation (35)

$$(\boldsymbol{q}_{n+1} - \boldsymbol{q}_j)^{\mathrm{T}} \left.\frac{\partial \mathcal{V}}{\partial \boldsymbol{q}}\right|_g^* + (\boldsymbol{q}_j - \boldsymbol{q}_n)^{\mathrm{T}} \left.\frac{\partial \mathcal{V}}{\partial \boldsymbol{q}}\right|_h^* + (\boldsymbol{q}_j - \boldsymbol{q}_n)^{\mathrm{T}} \frac{1}{2}\alpha \left[\left.\frac{\partial \mathcal{V}}{\partial \boldsymbol{q}}\right|_j - \left.\frac{\partial \mathcal{V}}{\partial \boldsymbol{q}}\right|_n \right]$$
$$= (\mathcal{V}_{n+1} - \mathcal{V}_j) + (\mathcal{V}_j - \mathcal{V}_n) + (\boldsymbol{q}_j - \boldsymbol{q}_n)^{\mathrm{T}} \frac{1}{2}\alpha \left[\left.\frac{\partial \mathcal{V}}{\partial \boldsymbol{q}}\right|_j - \left.\frac{\partial \mathcal{V}}{\partial \boldsymbol{q}}\right|_n \right].$$

In the RHS are identified the potential energy jump over the time-step $[t_n, t_{n+1}]$ plus the *potential energy of the jump*, that in order to be positive must also satisfy the local convexity

expressed in Equation (36). The constraint and gyroscopic forces are treated in the same way as in the previous section, i.e., the work done by them is null.

Finally, the change of the total energy has the expression:

$$\mathcal{K}_{n+1} - \mathcal{K}_n + \alpha\mathcal{K}_{nj} + \mathcal{V}_{n+1} - \mathcal{V}_n + \alpha\mathcal{V}_{nj} = \mathcal{E}_{n+1} - \mathcal{E}_n + \alpha(\mathcal{K}_{nj} + \mathcal{V}_{nj}) = 0 \tag{52}$$

from which

$$\mathcal{E}_{n+1} = \mathcal{E}_n - \alpha c^2 \quad c^2 \geq 0 \longrightarrow \mathcal{E}_{n+1} \leqq \mathcal{E}_n. \tag{53}$$

For $\alpha = 0$, an energy preserving scheme is obtained (note that it is different from that of Section 4), while for $\alpha = 1$ the maximum energy dissipation is reached. Note also that the energy decaying scheme presented in the previous section is recovered for $\alpha = 1$.

5.2.3 Numerical examples

The performance of the algorithm will be shown by analyzing the responses computed for the simple and double pendulums.

Figure 14 plots the simple pendulum displacements responses for the case $\alpha = 0$ for both models, *a* and *b*, whereas Figure 15 displays their velocities time responses. Clearly, the responses computed for both models differ completely, and a locking phenomenon can be observed in the constrained model.

This locking is also observed in the responses computed in the double-pendulum test cases (constrained models). In all cases, the total energy is perfectly preserved for the energy preserving scheme (Figure 16).

Figure 17 shows the amount of dissipation changes for different values of the parameter α for the simple pendulum. In the constrained model, the greatest amount of dissipation is not obtained for a value of $\alpha = 1$, as is the case for the unconstrained model. Moreover, the energy decays almost 10,000 times more for the constrained case than in the unconstrained one.

5.2.4 Discussion

In this section, a scheme with an algorithmic control of the amount of dissipated energy was introduced. This control works well only for unconstrained problems and for linearly constrained cases (although not shown here for brevity). The amount of dissipation increases monotonously with α from 0 to 1 in these cases. However, a locking phenomenon appears for nonlinearly constrained systems with $\alpha = 0$, and an excessive dissipation is reached when $\alpha \neq 0$. These problems are related to the independent interpolation fields of displacements and velocities, with a drift of constraints at the velocity level.

5.3 Energy decaying scheme with velocity constraints: $\alpha - \kappa$ algorithm

In order to avoid the numerical troubles of the previous scheme, it will be reformulated using the constraint stabilization technique proposed by Gear et al. [29–31], with a reduction of the governing DAEs from index 3 to index 2. The idea is to introduce a new algebraic constraint equation $\boldsymbol{B}\boldsymbol{L}^{-1}\boldsymbol{v} = \boldsymbol{0}$ with an associated Lagrange multiplier $\boldsymbol{\eta}$. By applying the Hamilton's principle in the same way as was done in Section 2, the new motion equations will result

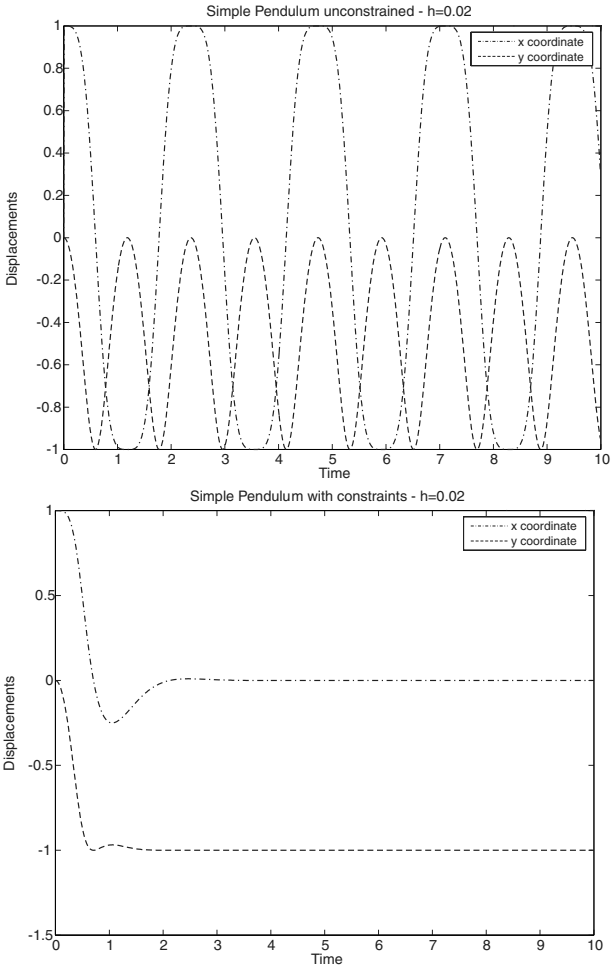

Fig. 14 Simple pendulum: displacements for test cases *a* and *b* in Cartesian coordinates (energy-decaying integration scheme with dissipation control)

from:

$$\delta \int_{t_1}^{t_2} \{\mathcal{L} - \boldsymbol{\mu}^{\mathrm{T}}(\boldsymbol{v} - \boldsymbol{L}\dot{\boldsymbol{q}}) - \boldsymbol{\lambda}^{\mathrm{T}}\boldsymbol{\Phi} - \boldsymbol{\eta}^{\mathrm{T}}\boldsymbol{B}\boldsymbol{L}^{-1}\boldsymbol{v}\}dt = 0. \tag{54}$$

Performing the variation on the variable $\boldsymbol{v}$, we can have

$$\boldsymbol{\mu} = \boldsymbol{M}\boldsymbol{v} - \boldsymbol{L}^{-\mathrm{T}}\boldsymbol{B}^{\mathrm{T}}\boldsymbol{\eta}. \tag{55}$$

Now introducing this expression in Equation (54) and with the help of Equation (3):

$$\delta \int_{t_1}^{t_2} \left\{ -\frac{1}{2}\boldsymbol{v}^{\mathrm{T}}\boldsymbol{M}\boldsymbol{v} - \mathcal{V}(\boldsymbol{q}) + \boldsymbol{v}^{\mathrm{T}}\boldsymbol{M}\boldsymbol{L}\dot{\boldsymbol{q}} - \boldsymbol{\lambda}^{\mathrm{T}}\boldsymbol{\Phi} - \boldsymbol{\eta}^{\mathrm{T}}\boldsymbol{B}\boldsymbol{L}^{-1}\boldsymbol{v} \right\} dt = 0. \tag{56}$$

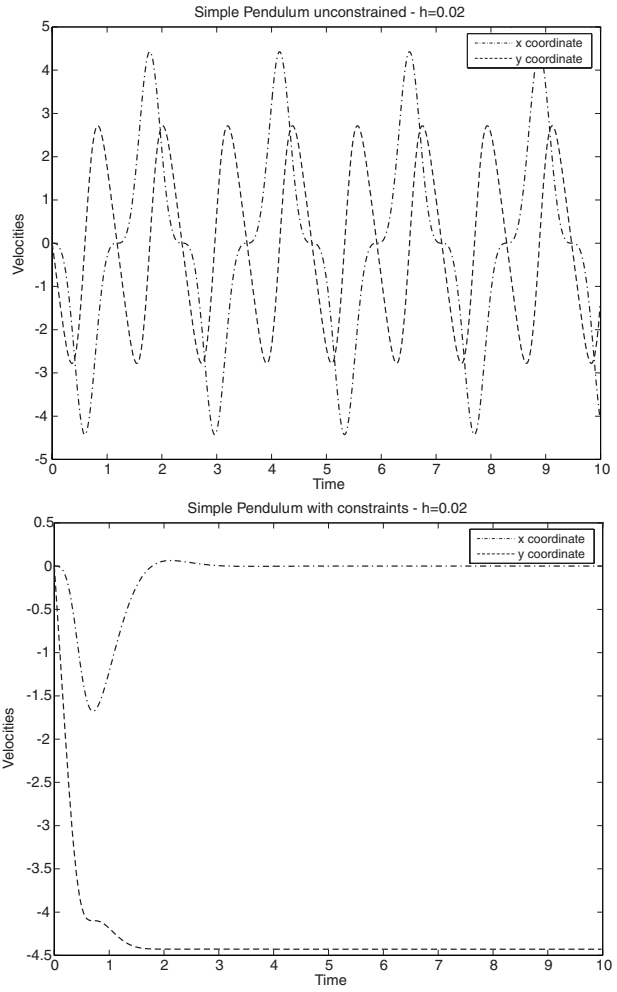

Fig. 15 Simple pendulum: velocities for test cases *a* and *b* in Cartesian coordinates (energy-decaying integration scheme with dissipation control)

This is the expression of the Hamilton's principle from which the motion equations will be derived. Now, performing the variation on the variables $\boldsymbol{v}$, $\boldsymbol{\lambda}$, $\boldsymbol{\eta}$, and $\boldsymbol{q}$ successively:

– variation of $\boldsymbol{v}$ yields

$$-\boldsymbol{M}\boldsymbol{v} + \boldsymbol{M}\boldsymbol{L}\dot{\boldsymbol{q}} - \boldsymbol{L}^{-\mathrm{T}}\boldsymbol{B}^{\mathrm{T}}\boldsymbol{\eta} = \boldsymbol{0} \tag{57}$$

– variation of the multipliers $\boldsymbol{\lambda}$ restores the constraints set (1)
– variation of the multipliers $\boldsymbol{\eta}$ gives

$$\boldsymbol{B}\boldsymbol{L}^{-1}\boldsymbol{v} = \boldsymbol{0} \tag{58}$$

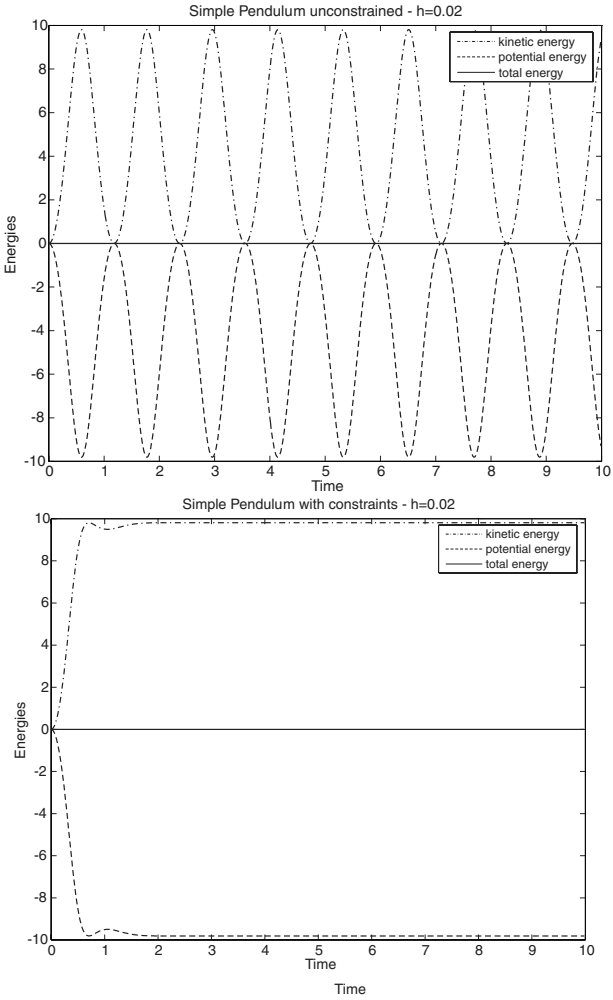

Fig. 16 Simple pendulum: kinetic, potential, and total energy for test cases *a* and *b* (energy decaying integration scheme with dissipation control)

– variation of the generalized displacements $\boldsymbol{q}$ yields

$$\int_{t_1}^{t_2} \left\{ -\frac{\partial \mathcal{V}}{\partial \boldsymbol{q}}\delta\boldsymbol{q} - \left(\frac{\partial \boldsymbol{\Phi}}{\partial \boldsymbol{q}}\right)^{\mathrm{T}} \boldsymbol{\lambda} + \delta\dot{\boldsymbol{q}}(\boldsymbol{L}^{\mathrm{T}}\boldsymbol{M}\boldsymbol{v}) + \delta\boldsymbol{q}\frac{\partial}{\partial \boldsymbol{q}}[(\boldsymbol{L}\dot{\boldsymbol{q}})^{\mathrm{T}}\boldsymbol{M}\boldsymbol{v}] \right\} dt = 0 \tag{59}$$

from which the dynamic equilibrium equations will be extracted.

Integration by parts of Equation (59) yields

$$\boldsymbol{L}^{\mathrm{T}}\boldsymbol{M}\dot{\boldsymbol{v}} + \boldsymbol{G}(\boldsymbol{M}\boldsymbol{v})\dot{\boldsymbol{q}} + \frac{\partial \mathcal{V}}{\partial \boldsymbol{q}} + \boldsymbol{B}^{\mathrm{T}}\boldsymbol{\lambda} = \boldsymbol{0}. \tag{60}$$

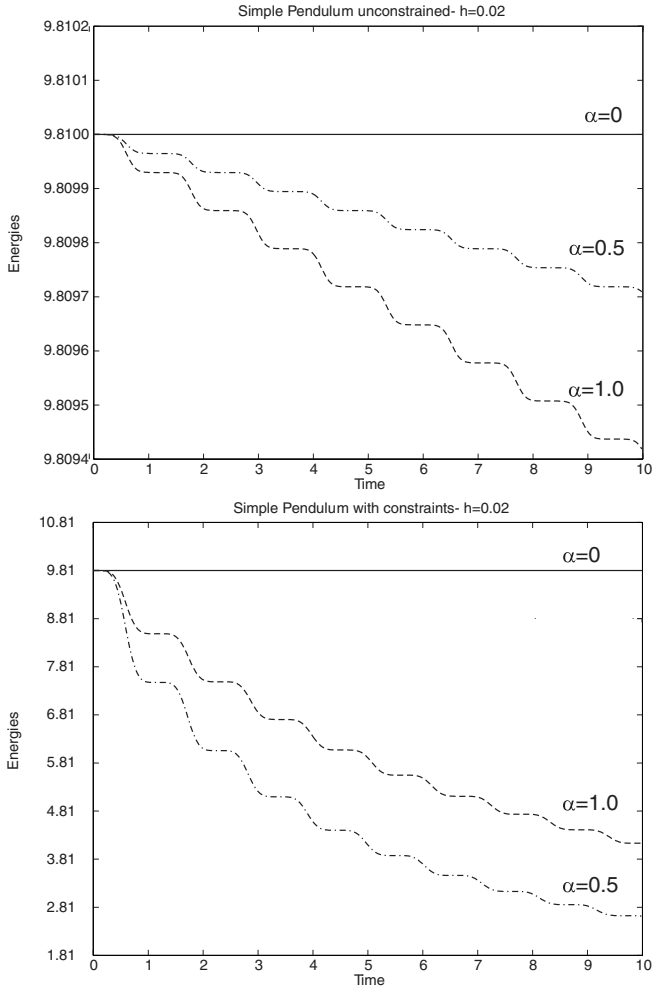

Fig. 17 Simple pendulum: total energy for test cases *a* and *b* for different values of parameter α (energy-decaying integration scheme with dissipation control)

Then, the equations of motion become a first-order DAE system with variables $\boldsymbol{q}$, $\boldsymbol{v}$, $\boldsymbol{\lambda}$, and $\boldsymbol{\eta}$:

$$\begin{cases} \boldsymbol{L}^{\mathrm{T}}\boldsymbol{M}\dot{\boldsymbol{v}} + \boldsymbol{G}\dot{\boldsymbol{q}} + \dfrac{\partial \mathcal{V}}{\partial \boldsymbol{q}} + \boldsymbol{B}^{\mathrm{T}}\boldsymbol{\lambda} = \boldsymbol{0} \\ -\boldsymbol{L}^{\mathrm{T}}\boldsymbol{M}\boldsymbol{v} + \boldsymbol{L}^{\mathrm{T}}\boldsymbol{M}\boldsymbol{L}\dot{\boldsymbol{q}} - \boldsymbol{B}^{\mathrm{T}}\boldsymbol{\eta} = \boldsymbol{0} \\ \boldsymbol{\Phi} = \boldsymbol{0} \\ \boldsymbol{B}\boldsymbol{L}^{-1}\boldsymbol{v} = \boldsymbol{0}. \end{cases} \tag{61}$$

This formulation provides the automatic enforcement of the velocity-level constraint besides the position-level one, thus eliminating the problem of drift for these constraints.

5.3.1 Discretization of the equation of motion

The interpolated displacements and velocities have the same expressions as in the previous scheme:

$$\begin{aligned} \boldsymbol{q} &= \frac{(\boldsymbol{q}_j + \boldsymbol{q}_{n+1})}{2} + \tau \frac{(\boldsymbol{q}_{n+1} - \alpha \boldsymbol{q}_j - (1-\alpha)\boldsymbol{q}_n)}{2}, \quad \dot{\boldsymbol{q}} = \frac{(\boldsymbol{q}_{n+1} - \boldsymbol{q}_j)}{h} \\ \boldsymbol{v} &= \frac{(\boldsymbol{v}_j + \boldsymbol{v}_{n+1})}{2} + \tau \frac{(\boldsymbol{v}_{n+1} - \alpha \boldsymbol{v}_j - (1-\alpha)\boldsymbol{v}_n)}{2}, \quad \dot{\boldsymbol{v}} = \frac{(\boldsymbol{v}_{n+1} - \boldsymbol{v}_j)}{h}. \end{aligned} \tag{62}$$

In the same way, internal and constraint forces are interpolated:

$$\begin{aligned} \frac{\partial \mathcal{V}}{\partial \boldsymbol{q}} &= \left.\frac{\partial \mathcal{V}}{\partial \boldsymbol{q}}\right|_g + \frac{\tau}{2}\left[\left.\frac{\partial \mathcal{V}}{\partial \boldsymbol{q}}\right|_{n+1} - \alpha \left.\frac{\partial \mathcal{V}}{\partial \boldsymbol{q}}\right|_j - (1-\alpha) \left.\frac{\partial \mathcal{V}}{\partial \boldsymbol{q}}\right|_n \right] \\ \boldsymbol{B}^{\mathrm{T}}\boldsymbol{\lambda} &= \boldsymbol{B}_g^{\mathrm{T}}\boldsymbol{\lambda}_g + \frac{\tau}{2}\left(\boldsymbol{B}_{n+1}^{\mathrm{T}}\boldsymbol{\lambda}_{n+1} - \boldsymbol{B}_j^{\mathrm{T}}\boldsymbol{\lambda}_j\right) \\ \boldsymbol{B}^{\mathrm{T}}\boldsymbol{\eta} &= \boldsymbol{B}_g^{\mathrm{T}}\boldsymbol{\eta}_g + \frac{\tau}{2}\left(\boldsymbol{B}_{n+1}^{\mathrm{T}}\boldsymbol{\eta}_{n+1} - \boldsymbol{B}_j^{\mathrm{T}}\boldsymbol{\eta}_j\right). \end{aligned} \tag{63}$$

The time-discontinuous Galerkin approximation of Equation (61) can be written as

$$\begin{aligned} &\int_{-1}^{1} \mathcal{W}_1(\tau)\left[\dot{\boldsymbol{q}} - \boldsymbol{L}^{-1}\boldsymbol{M}^{-1}\boldsymbol{L}^{-\mathrm{T}}\boldsymbol{B}^{\mathrm{T}}\boldsymbol{\eta} - \boldsymbol{L}^{-1}\boldsymbol{v}\right] d\tau \\ &\quad + \int_{-1}^{1} \mathcal{W}_2(\tau)\left[\boldsymbol{M}\dot{\boldsymbol{v}} + \boldsymbol{L}^{-\mathrm{T}}\boldsymbol{G}\dot{\boldsymbol{q}} + \boldsymbol{L}^{-\mathrm{T}}\boldsymbol{B}^{\mathrm{T}}\boldsymbol{\lambda} + \boldsymbol{L}^{-\mathrm{T}}\frac{\partial \mathcal{V}}{\partial \boldsymbol{q}}\right] d\tau \\ &\quad + \mathcal{W}_1(-1)(\boldsymbol{q}_j - \boldsymbol{q}_n) + \mathcal{W}_2(-1)[\boldsymbol{M}(\boldsymbol{v}_j - \boldsymbol{v}_n) + \boldsymbol{L}^{-\mathrm{T}}\boldsymbol{G}_h(\boldsymbol{q}_j - \boldsymbol{q}_n)] = 0, \end{aligned} \tag{64}$$

where

$$\mathcal{W}_1(\tau) = A_1 + B_1\tau, \quad \mathcal{W}_2(\tau) = A_2 + B_2\tau. \tag{65}$$

Integration of this expression leads to the discrete equations system formed by the equilibrium equations, the velocities/displacements relationships, and the constraints at

displacement-level and at velocity-level:

$$
\begin{cases}
\dfrac{1}{h}\boldsymbol{L}^{\mathrm{T}}\boldsymbol{M}(\boldsymbol{v}_{n+1}-\boldsymbol{v}_n)+\dfrac{1}{h}\boldsymbol{G}_m(\boldsymbol{q}_{n+1}-\boldsymbol{q}_n)+\left.\dfrac{\partial\mathcal{V}}{\partial\boldsymbol{q}}\right|_g+(\boldsymbol{B}^{\mathrm{T}}\boldsymbol{\lambda})_g=\boldsymbol{0}\\
\dfrac{1}{h}\boldsymbol{L}^{\mathrm{T}}\boldsymbol{M}(\boldsymbol{v}_j-\boldsymbol{v}_n)+\dfrac{1}{h}\boldsymbol{G}_h(\boldsymbol{q}_j-\boldsymbol{q}_n)-\dfrac{1}{3}\left[\left.\dfrac{\partial\mathcal{V}}{\partial\boldsymbol{q}}\right|_g-\left.\dfrac{\partial\mathcal{V}}{\partial\boldsymbol{q}}\right|_h\right]\\
\quad+\dfrac{1}{6}\alpha\left[\left.\dfrac{\partial\mathcal{V}}{\partial\boldsymbol{q}}\right|_j-\left.\dfrac{\partial\mathcal{V}}{\partial\boldsymbol{q}}\right|_n\right]-\dfrac{1}{3}\left(\boldsymbol{B}_g^{\mathrm{T}}\boldsymbol{\lambda}_g-\boldsymbol{B}_h^{\mathrm{T}}\boldsymbol{\lambda}_j\right)=\boldsymbol{0}\\
\dfrac{1}{h}\boldsymbol{L}^{\mathrm{T}}\boldsymbol{M}\boldsymbol{L}(\boldsymbol{q}_{n+1}-\boldsymbol{q}_n)-\dfrac{\kappa}{2}\left(\boldsymbol{B}_{n+1}^{\mathrm{T}}\boldsymbol{\eta}_{n+1}+\boldsymbol{B}_j^{\mathrm{T}}\boldsymbol{\eta}_j\right)-\dfrac{\kappa}{2}\boldsymbol{L}^{\mathrm{T}}\boldsymbol{M}(\boldsymbol{v}_{n+1}+\boldsymbol{v}_j)=\boldsymbol{0}\\
\dfrac{1}{h}\boldsymbol{L}^{\mathrm{T}}\boldsymbol{M}\boldsymbol{L}(\boldsymbol{q}_j-\boldsymbol{q}_n)+\dfrac{\kappa}{6}\left(\boldsymbol{B}_{n+1}^{\mathrm{T}}\boldsymbol{\eta}_{n+1}-\boldsymbol{B}_j^{\mathrm{T}}\boldsymbol{\eta}_j\right)\\
\quad+\dfrac{\kappa}{6}\boldsymbol{L}^{\mathrm{T}}\boldsymbol{M}(\boldsymbol{v}_{n+1}-\alpha\boldsymbol{v}_j-(1-\alpha)\boldsymbol{v}_n)=\boldsymbol{0}\\
\boldsymbol{\Phi}_j=\boldsymbol{0}\\
\boldsymbol{\Phi}_{n+1}=\boldsymbol{0}\\
\boldsymbol{B}_j\boldsymbol{L}^{-1}\boldsymbol{v}_j=\boldsymbol{0}\\
\boldsymbol{B}_{n+1}\boldsymbol{L}^{-1}\boldsymbol{v}_{n+1}=\boldsymbol{0}
\end{cases}
\tag{66}
$$

for $0\leq\alpha\leq 1$.

An algorithmic parameter κ was introduced, which will be adjusted following the criterion of verifying energy preservation in the case $\alpha=0$, as is shown in the next section. This parameter should be $\kappa=1+O(h)$, that is,

$$
\lim_{h\to 0}\kappa=1 \tag{67}
$$

for consistency. For $\alpha=0$, the scheme preserves the total energy of the system (depending on the value of κ) and for $\alpha=1$ it reaches the maximum energy dissipation.

5.3.2 Energy decay in the discrete scheme – computation of κ

The free parameter κ is computed by asking that in the case $\alpha=0$ the total energy of the system should be preserved. This idea leads to an equation that gives the value to be used at each time step.

Let us premultiply Equation (66a) by $(\boldsymbol{q}_{n+1}-\boldsymbol{q}_n)^{\mathrm{T}}$, Equation (66b) by $(\boldsymbol{q}_j-\boldsymbol{q}_n)^{\mathrm{T}}$, Equation (66c) by $(\boldsymbol{v}_{n+1}-\boldsymbol{v}_n)^{\mathrm{T}}\boldsymbol{L}^{-1}$, and Equation (66d) by $(\boldsymbol{v}_j-\boldsymbol{v}_n)^{\mathrm{T}}\boldsymbol{L}^{-1}$. Combining linearly these four equations and after some algebraic manipulations:

$$
\begin{aligned}
&\frac{\kappa}{2}\left(\boldsymbol{v}_{n+1}^{\mathrm{T}}\boldsymbol{M}\boldsymbol{v}_{n+1}-\boldsymbol{v}_n^{\mathrm{T}}\boldsymbol{M}\boldsymbol{v}_n\right)\\
&\quad+\frac{\kappa\alpha}{2}\left(\boldsymbol{v}_j^{\mathrm{T}}\boldsymbol{M}\boldsymbol{v}_j-\boldsymbol{v}_j^{\mathrm{T}}\boldsymbol{M}\boldsymbol{v}_n-\boldsymbol{v}_n^{\mathrm{T}}\boldsymbol{M}\boldsymbol{v}_j+\boldsymbol{v}_n^{\mathrm{T}}\boldsymbol{M}\boldsymbol{v}_n\right)
\end{aligned}
$$

$$
\begin{aligned}
&+(\boldsymbol{q}_{n+1}-\boldsymbol{q}_j)^{\mathrm{T}}\left.\frac{\partial \mathcal{V}}{\partial \boldsymbol{q}}\right|_g+(\boldsymbol{q}_j-\boldsymbol{q}_n)^{\mathrm{T}}\left.\frac{\partial \mathcal{V}}{\partial \boldsymbol{q}}\right|_h+(\boldsymbol{q}_j-\boldsymbol{q}_n)^{\mathrm{T}}\frac{\alpha}{2}\left[\left.\frac{\partial \mathcal{V}}{\partial \boldsymbol{q}}\right|_j-\left.\frac{\partial \mathcal{V}}{\partial \boldsymbol{q}}\right|_n\right]\\
&+(\boldsymbol{q}_{n+1}-\boldsymbol{q}_j)^{\mathrm{T}}\boldsymbol{B}_g^{\mathrm{T}}\boldsymbol{\lambda}_g+(\boldsymbol{q}_j-\boldsymbol{q}_n)^{\mathrm{T}}\boldsymbol{B}_h^{\mathrm{T}}\boldsymbol{\lambda}_j\\
&+\frac{\kappa}{2}(\boldsymbol{v}_{n+1}-\boldsymbol{v}_n)^{\mathrm{T}}\boldsymbol{L}^{-1}(\boldsymbol{B}_{n+1}\boldsymbol{\eta}_{n+1}+\boldsymbol{B}_j\boldsymbol{\eta}_j)\\
&-\frac{\kappa}{2}(\boldsymbol{v}_j-\boldsymbol{v}_n)^{\mathrm{T}}\boldsymbol{L}^{-1}\big(\boldsymbol{B}_{n+1}^{\mathrm{T}}\boldsymbol{\eta}_{n+1}-\boldsymbol{B}_j^{\mathrm{T}}\boldsymbol{\eta}_j\big)=0.
\end{aligned}
\tag{68}
$$

The work done by the gyroscopic forces is null because of the skew-symmetry of $\boldsymbol{G}_m$ and $\boldsymbol{G}_h$, as was reported in the previous sections.

By identifying the different energy terms and grouping them together:

$$
\begin{aligned}
&\kappa\left[\mathcal{K}_{n+1}-\mathcal{K}_n+\frac{\alpha}{2}(\boldsymbol{v}_j-\boldsymbol{v}_n)^{\mathrm{T}}\boldsymbol{M}(\boldsymbol{v}_j-\boldsymbol{v}_n)\right]\\
&\quad+\mathcal{V}_{n+1}-\mathcal{V}_n+(\boldsymbol{q}_j-\boldsymbol{q}_n)^{\mathrm{T}}\frac{\alpha}{2}\left[\left.\frac{\partial \mathcal{V}}{\partial \boldsymbol{q}}\right|_j-\left.\frac{\partial \mathcal{V}}{\partial \boldsymbol{q}}\right|_n\right]\\
&\quad+\frac{\kappa}{2}(\boldsymbol{v}_{n+1}-\boldsymbol{v}_n)^{\mathrm{T}}\boldsymbol{L}^{-1}(\boldsymbol{B}_{n+1}\boldsymbol{\eta}_{n+1}+\boldsymbol{B}_j\boldsymbol{\eta}_j)\\
&\quad-\frac{\kappa}{2}(\boldsymbol{v}_j-\boldsymbol{v}_n)^{\mathrm{T}}\boldsymbol{L}^{-1}(\boldsymbol{B}_{n+1}^{\mathrm{T}}\boldsymbol{\eta}_{n+1}-\boldsymbol{B}_j^{\mathrm{T}}\boldsymbol{\eta}_j)=0,
\end{aligned}
\tag{69}
$$

where the concept of *discrete directional derivative* has been used again as was done in the previous sections, replacing the expressions $(\partial\mathcal{V}/\partial\boldsymbol{q})_g$ and $(\partial\mathcal{V}/\partial\boldsymbol{q})_h$ by the discrete counterparts that verify the expressions (35). Matrices $\boldsymbol{B}_g$ and $\boldsymbol{B}_h$ were approximated with $\boldsymbol{B}_g^*$ and $\boldsymbol{B}_h^*$ in order to satisfy Equation (37).

Now, for $\alpha=0$, the algorithmic total energy of the system must be perfectly preserved, that is:

$$
\begin{aligned}
&(\mathcal{V}_{n+1}-\mathcal{V}_n)+\kappa(\mathcal{K}_{n+1}-\mathcal{K}_n)\\
&\quad+\frac{\kappa}{2}\left[\boldsymbol{\eta}_j^{\mathrm{T}}\boldsymbol{B}_j\boldsymbol{L}^{-1}(\boldsymbol{v}_{n+1}+\boldsymbol{v}_j-2\boldsymbol{v}_n)+\boldsymbol{\eta}_{n+1}^{\mathrm{T}}\boldsymbol{B}_{n+1}\boldsymbol{L}^{-1}(\boldsymbol{v}_{n+1}-\boldsymbol{v}_j)\right]=\boldsymbol{0}.
\end{aligned}
\tag{70}
$$

Then, a closed form to compute the κ coefficient is obtained:

$$
\kappa=1-\frac{\boldsymbol{\eta}_j^{\mathrm{T}}\boldsymbol{B}_j\boldsymbol{L}^{-1}(\boldsymbol{v}_{n+1}+\boldsymbol{v}_j-2\boldsymbol{v}_n)+\boldsymbol{\eta}_{n+1}^{\mathrm{T}}\boldsymbol{B}_{n+1}\boldsymbol{L}^{-1}(\boldsymbol{v}_{n+1}-\boldsymbol{v}_j)}{2(\mathcal{K}_{n+1}-\mathcal{K}_n)+\boldsymbol{\eta}_j^{\mathrm{T}}\boldsymbol{B}_j\boldsymbol{L}^{-1}(\boldsymbol{v}_{n+1}+\boldsymbol{v}_j-2\boldsymbol{v}_n)+\boldsymbol{\eta}_{n+1}^{\mathrm{T}}\boldsymbol{B}_{n+1}\boldsymbol{L}^{-1}(\boldsymbol{v}_{n+1}-\boldsymbol{v}_j)}.
\tag{71}
$$

It can be seen that κ is 1 minus a measure of the work done by the constraint forces at the velocity level with respect to the kinetic energy jump.

5.3.3 Remarks

- The computation of the algorithmic parameter κ is based on requiring the integrator to be conservative for $\alpha=0$. A similar technique was proposed by Simo [8] and Betsch and Steinmann [14], with the difference that in those cases this technique was used to enforce the energy preservation at all levels, while in the present proposal the technique is applied

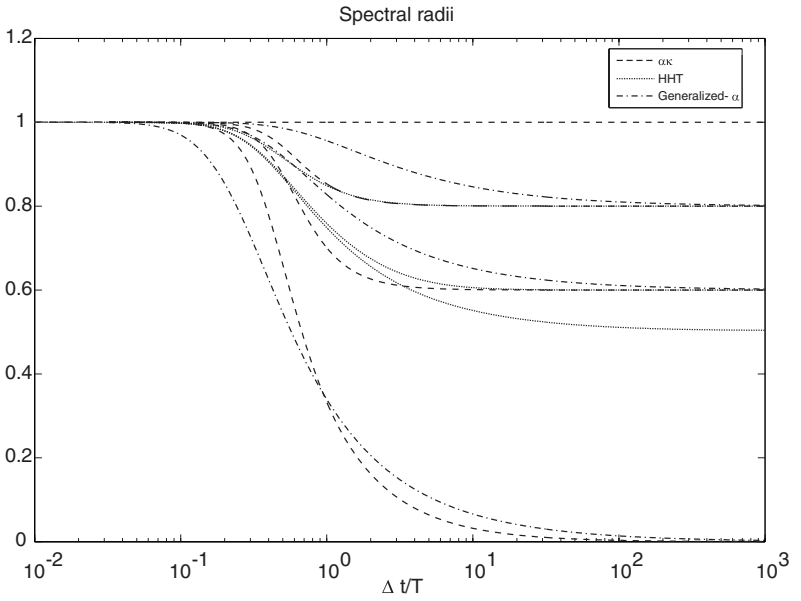

Fig. 18 Comparison of spectral radii of numerical dissipative algorithms

only for compensating the energy contribution of the velocity-level constraint forces. This technique has also been used recently by Pfeiffer and Arnold [32] for Hamiltonian systems.

– The denominator in Equation (71) is not guaranteed to be different from zero at every step. Therefore, the scheme may face troubles when this term is close to zero. This aspect deserves further study to determine the influence it can have on the computations.
– The algorithmic parameter κ should be $1 + O(h)$ for consistency. In most cases, the increment in the work of the constraint forces at velocity level is much smaller than the kinetic energy jump, thus satisfying this requirement. However, at steps in which the denominator of Equation (71) is small, this condition could be violated. In order to avoid this inconvenience, in our experiments we limited the value of κ to lie within the interval $[1 - h/2, 1 + h/2]$. In this way, the energy preservation was not exactly verified at every time instant, and at certain time steps a slight energy drift was observed. However, this energy drift was small since the contribution of the velocity-level forces of constraint is much smaller than the leading energy terms.
– An alternative is simply to keep the value of κ constant and equal to 1. The resulting scheme is not conservative for $\alpha = 0$, but it still verifies that for increasing values of α the amount of dissipation increases monotonously (see Equation (69), where the α factors are the positive definite kinetic and deformation energies of the jump). As pointed out in the preceding remark, the energy drift introduced by the forces of constraint at the velocity level is much smaller than the leading energy terms, which verify preservation.
– It should be noted that the equations of motion should be properly scaled to avoid ill conditioning of the equations when the time step is decreased [33, 34].

5.3.4 Algorithm properties

Several properties of the algorithm, such as its stability and accuracy properties in the linear range, can be studied by a conventional analysis based on the characteristics of the

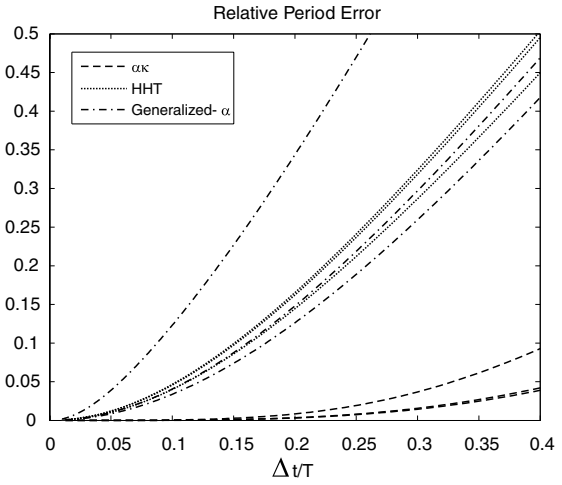

Fig. 19 Relative period errors of time integration algorithms

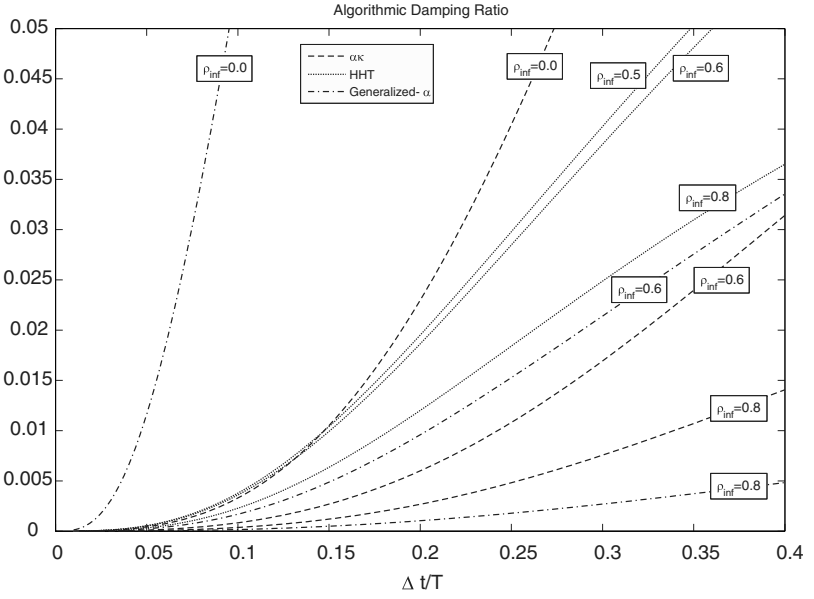

Fig. 20 Algorithmic damping ratios of numerically dissipative algorithms

amplification matrix. Let us consider a one degree-of-freedom linear oscillator of natural frequency ω:

$$\ddot{q} + \omega^2 q = 0, \tag{72}$$

and solve this equation numerically with our algorithm with time-step h.

The spectral radius, relative period errors, and algorithmic damping are shown in Figures 18–20, respectively, as a function of $h/T = \omega h/(2\pi)$. The results are compared with those given by generalized-α [2] and HHT [1] methods, for three different values of spectral radius at infinity: $\rho_\infty = 0.6, 0.8$ and the value of maximum dissipation for each scheme, i.e.,

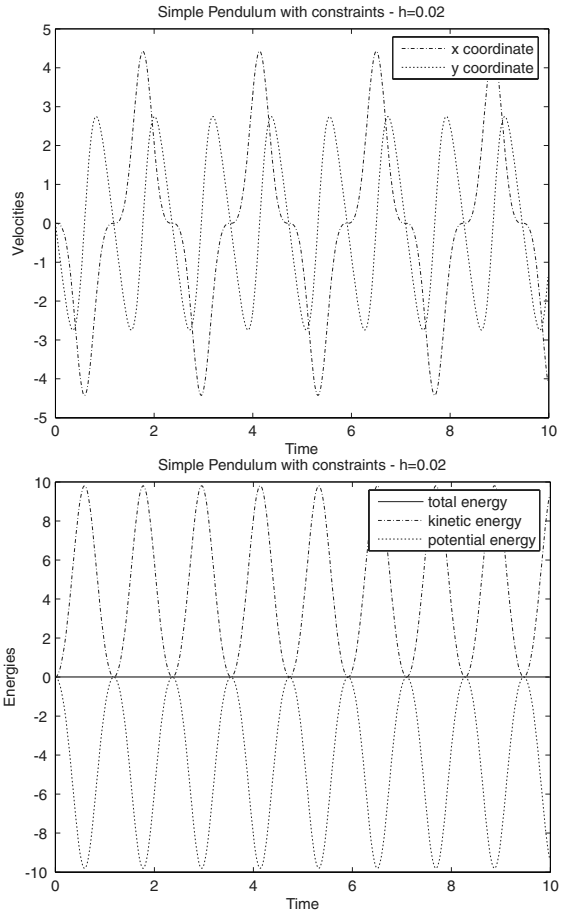

Fig. 21 Simple pendulum: velocities and energies in Cartesian coordinates for test case b and $\alpha = 0$ ($\alpha - \kappa$ integration scheme)

$\rho_\infty = 0.5$ for the HHT and $\rho_\infty = 0$ for the two others. Figure 19 shows that the algorithm $\alpha - \kappa$ has the smallest period error, for any value of α. Asymptotic annihilation is achieved with the $\alpha - \kappa$ scheme and the unconditional stability is ensured because the spectral radius is always smaller than unity.

5.3.5 Numerical examples

Figure 21 shows that now this scheme works well in the constrained case (it does so also for the unconstrained case). The locking problem has disappeared. In addition, the amount of energy dissipated increases monotonously with α and its values are now 1000 times lower than before for the case of $\alpha = 1$ (Figure 22).

Figure 23 shows a plot of the evolution of the parameter κ, for an integration performed with $\alpha = 0$, using a time-step size $h = 0.02$. We can see that the consistency requirement of having κ close to 1 was clearly verified in this example.

The convergence of the algorithm for the simple pendulum problem is plotted in Figure 24, where the second order of convergence for the displacements and the first order for the Lagrange multiplier λ_g can be observed.

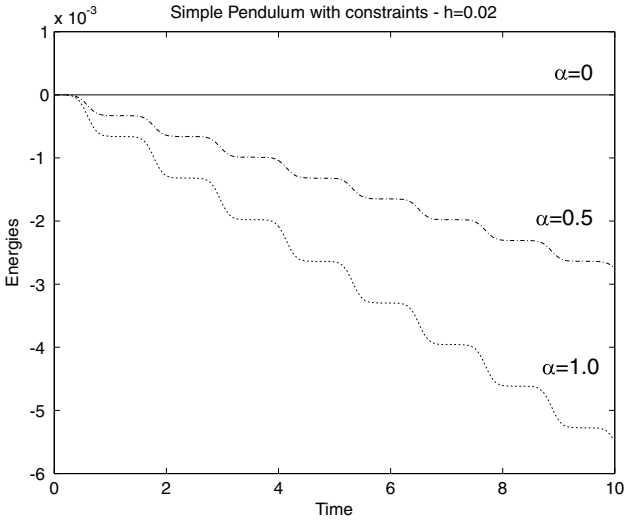

Fig. 22 Simple pendulum: time evolution of total energy for different values of α for the test-case b ($\alpha - \kappa$ integration scheme)

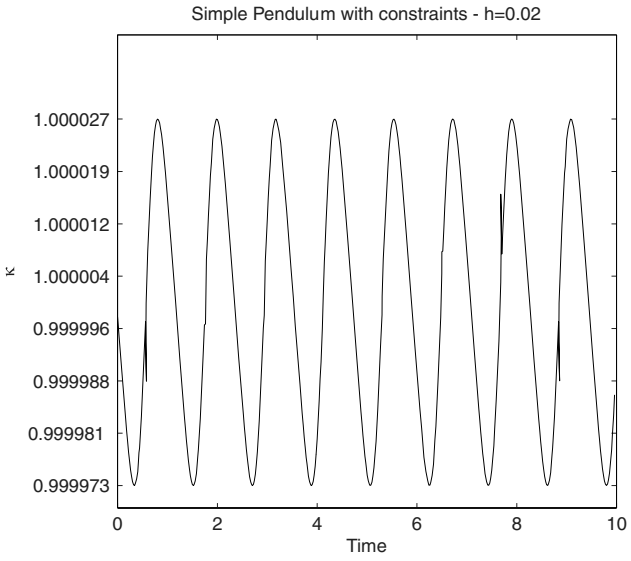

Fig. 23 Simple pendulum: time evolution of κ coefficient with $\alpha = 0$ for the test-case b ($\alpha - \kappa$ integration scheme)

Figures 25 and 26 plot the time responses for the test case d, in which κ was kept constant equal to one ($\kappa = 1$) and the energy dissipation was maximized by setting $\alpha = 1$. The time step used in this analysis was $h = 0.01$. It should be noted that when using the energy preserving scheme, it was not possible to perform the analysis with a time step higher than $h = 0.001$ because of the violent velocity oscillations (Figure 8). This algorithm was able to

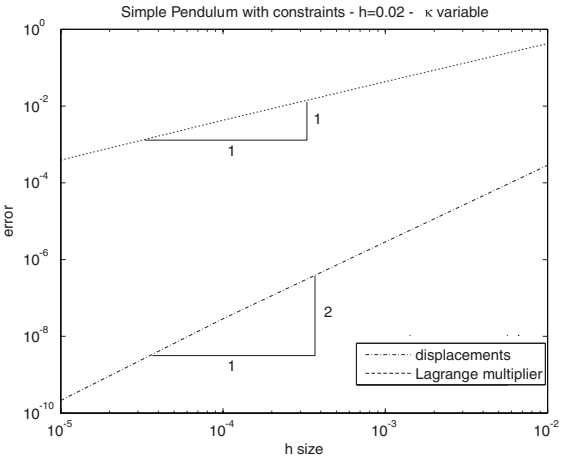

Fig. 24 Analysis of convergence in the simple pendulum test case. A quadratic convergence rate is observed for the displacements and a linear convergence rate for the Lagrange multipliers

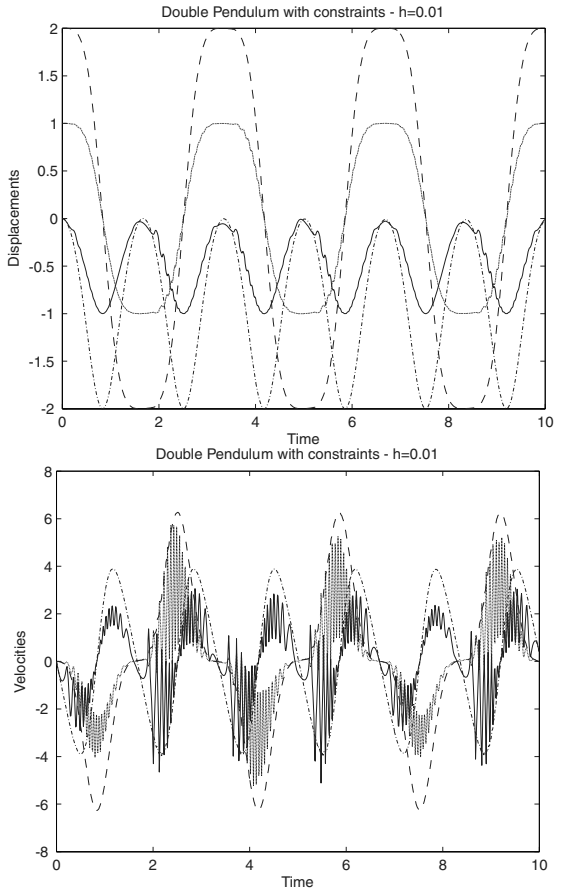

Fig. 25 Double pendulum: time responses for displacements and velocities for $m_1 = 0.005$ and $m_2 = 1$, test-case d ($\alpha - \kappa$ integration scheme), with $h = 0.01$. The algorithm parameter is kept constant ($\kappa = 1$) and the energy dissipation is maximized ($\alpha = 1$)

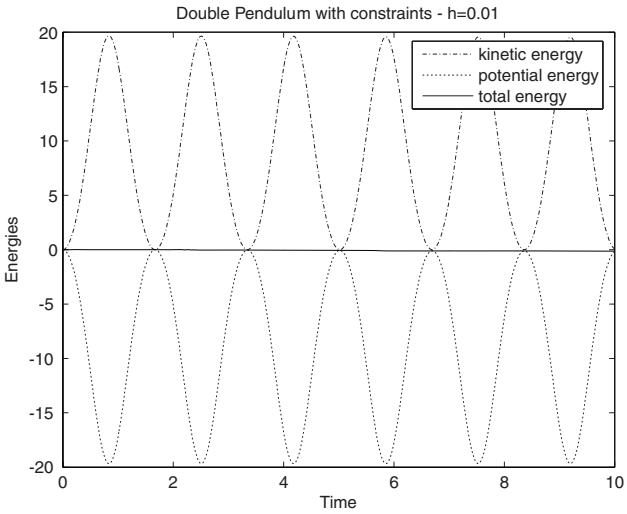

Fig. 26 Double pendulum: time responses for kinetic, potential, and total energy for $m_1 = 0.005$ and $m_2 = 1$, test-case d ($\alpha - \kappa$ integration scheme), with $h = 0.01$, $\kappa = 1$, and $\alpha = 1$

solve the same test case by using a time step which was 10 times higher than with the energy preserving scheme.

6 Concluding remarks

A variety of time integration schemes for constrained multibody dynamics were analyzed.

It has been shown that although the energy preserving scheme provides nonlinear unconditional stability for MBS, it lacks high-frequency numerical dissipation without which many time algorithms can lead to the damage of the computation in realistic engineering problems.

The high-frequency numerical dissipation is therefore imperative for time integration of multibody systems in order to assure the stability of the solution, and it was demonstrated that it can be obtained using schemes with independent interpolation of displacements and velocities. It was demonstrated that not only constraints but also the time derivatives of constraints should be imposed when using independent interpolation of displacements and velocities to avoid locking. A new algorithm was proposed based on this idea, that meets specific requirements of unconditionally stable integration in constrained nonlinear elastodynamics, energy dissipation with control of the asymptotic spectral radius, capability of handling nonlinear constraints, capability of handling large finite rotations, and continuous variation of the asymptotic spectral radius varying from energy preservation up to total annihilation. In order to achieve these properties, a discretization process was developed for elastic and inertial forces to obtain the corresponding preservation or dissipation of the total mechanical energy of the system at the discrete solution level. A discretization process was developed also for the constraint forces, so as to guarantee the exact satisfaction of nonlinear constraints and the exact vanishing of their work.

The performance of the proposed algorithm was demonstrated with a series of numerical tests covering the most important characteristics of numerical models of MBS.

Acknowledgements The authors wish to thank the reviewers for their most valuable comments. Financial support from Agencia Nacional de Promoción Científica y Tecnológica, Argentina, through Grants PID 99-76 and PID 03-398, and from Universidad Nacional del Litoral, through Grant CAI + D PE 214, is gratefully acknowledged.

References

1. Cardona, A.: An Integrated Approach to Mechanism Analysis. Ph.D. thesis, Faculté des Sciences Appliquées, Université of Liège, Belgique (1989)
2. Chung, J., Hulbert, G.M.: A time integration algorithm for structural dynamics with improved numerical dissipation: the generalized α method. J. Appl. Mech. **60**, 371–375 (1993)
3. Hughes, T.J.R.: Analysis of transient algorithms with particular reference to stability behaviour. In: Computational Methods for Transient Analysis. Belytschko, T., Hughes, T.J.R. (eds.), North-Holland, Amsterdam (1983)
4. Haug, E., Nguyen, O.S., Rouvray, A.L.: An improved energy conserving implicit time integration algorithm for nonlinear dynamic structural analysis. In: Proceedings of the Fourth Conference on Structural Mechanics in Reactor Technology, San Francisco, CA, August (1977)
5. Hughes, T.J.R., Liu, W.K., Caughey, T.K.: Finite-element methods for nonlinear elastodynamics which conserve energy. J. Appl. Mech. **45**, 366–370 (1978)
6. Bottasso, C., Trainelli, L.: An attempt at the classification of energy decaying schemes for structural and multibody dynamics. Multibody Syst. Dyn. **12**, 173–185 (2004)
7. Simo, J.C., Wong, K.K.: Unconditionally stable algorithms for rigid body dynamics that exactly preserve energy and momentum. Int. J. Numer. Methods Eng. **31**, 19–52 (1991)
8. Simo, J.C., Tarnow, N., Wong, K.K.: Exact energy–momentum conserving algorithms and symplectic schemes for nonlinear dynamics. Comput. Methods Appl. Mech. Eng. **100**, 63–116 (1992)
9. Simo, J.C., Tarnow, N.: The discrete energy–momentum method. Conserving algorithms for nonlinear elastodynamics. Zeitschrift fuer Angewandte Mathematik und Physik (ZAMP) **43**, 757–792 (1992)
10. Simo, J.C., Tarnow, N., Doblare, M.: Non-linear dynamics of three-dimensional rods: exact energy and momentum conserving algorithms. Int. J. Numer. Methods Eng. **38**, 1431–1473 (1995)
11. Hilber, H.M., Hughes, T.J.R., Taylor, R.L.: Improved numerical dissipation for time integration algorithms in structural dynamics. Earthq. Eng. Struct. Dyn. **5**, 282–292 (1977)
12. Zienkiewicz, O.C., Wood, W.L., Taylor, R.L.: An alternative single-step algorithm for dynamic problems. Earthq. Eng. Struct. Dyn. **8**, 31–40 (1980)
13. Ibrahimbegovic, A., Mamouri, S., Taylor, R.L., Chen, J.A.: Finite element method in dynamics of flexible multibody systems: modelling of holonomic constraints and energy conserving integration schemes. Multibody Syst. Dyn. **4**, 195–223 (2000)
14. Betsch, P., Steinmann, P.: Conservation properties of a time FE method. Part I: Time-stepping schemes for n-body problems. Int. J. Numer. Methods Eng. **49**, 599–638 (2000)
15. Betsch, P., Steinmann, P.: Conservation properties of a time FE method. Part II: Time-stepping schemes for non-linear elastodynamics. Int. J. Numer. Methods Eng. **50**, 1931–1955 (2001)
16. Betsch, P., Steinmann, P.: Conservation properties of a time FE method. Part III: Mechanical systems with holonomic constraints. Int. J. Numer. Methods Eng. **53**, 2271–2304 (2002)
17. Betsch, P., Steinmann, P.: Constrained integration of rigid body dynamics. Comput. Methods Appl. Mech. Eng. **191**, 467–488 (2001)
18. Bauchau, O., Damilano, G., Theron, J.: Numerical integration of non-linear elastic multi-body systems. Int. J. Numer. Methods Eng. **38**, 2727–2751 (1995)
19. Géradin, M., Cardona, A.: Flexible Multibody Dynamics: A Finite Element Approach. Wiley, New York (2000)
20. Lens, E., Cardona, A., Géradin, M.: Energy preserving time integration for constrained multibody systems. Multibody Syst. Dyn. **11**, 41–61 (2004)
21. Johnson, C.: Numerical Solution of Partial Differential Equations by the Finite Element Method. Cambridge University Press, Cambridge, UK (1994)
22. Bauchau, O.: Computational schemes for flexible, non-linear multibody systems. Multibody Syst. Dyn. **2**, 169–225 (1998)
23. Bauchau, O., Joo, T.: Computational schemes for nonlinear elasto-dynamics. Int. J. Numer. Methods Eng. **45**, 693–719 (1999)
24. Armero, F., Romero, I.: On the formulation of high-frequency dissipative time-stepping algorithms for nonlinear dynamics. Part I: Low-order methods for two model problems and nonlinear elastodynamics. Comput. Methods Appl. Mech. Eng. **190**, 2603–2649 (2001)

25. Armero, F., Romero, I.: On the formulation of high-frequency dissipative time-stepping algorithms for nonlinear dynamics. Part II: Second-order methods. Comput. Methods Appl. Mech. Eng. **190**, 6783–6824 (2001)
26. Ibrahimbegovic, A., Mamouri, S.: Energy conserving/decaying implicit time-stepping scheme for nonlinear dynamics of three-dimensional beams undergoing finite rotations. Comput. Methods Appl. Mech. Eng. **191**, 4241–4258 (2002)
27. Ibrahimbegovic, A., Mamouri, S.: On rigid components and joint constraints in nonlinear dynamics of flexible multibody systems employing 3D geometrically exact beam model. Comput. Methods Appl. Mech. Eng. **188**, 805–831 (2000)
28. Gonzalez, O.: Mechanical systems subject to holonomic constraints: differential-algebraic formulations and conservative integration. Physica D **132**, 165–174 (1999)
29. Gear, C.W., Leimkuhler, B., Gupta, G.K.: Automatic integration of Euler–Lagrange equations with constraints. J. Comput. Appl. Math. **12–13**, 77–90 (1985)
30. Brennan, K.E., Campbell, S.L., Petzold, L.R.: Numerical Solution of Initial-Value Problems in Differential-Algebraic Equations. Elsevier, Amsterdam (1989)
31. Hairer, E., Wanner, G.: Solving Ordinary Differential Equations. II Stiff and Differential-Algebraic Problems. Springer-Verlag, Berlin (1996)
32. Pfeiffer, A., Arnold, M.: Numerical analysis of structure preserving Nyström methods for Hamiltonian systems. Appl. Numer. Math. **53**, 391–408 (2005)
33. Cardona, A., Géradin, M.: Numerical integration of second-order differential-algebraic systems in flexible mechanism dynamics. In: Computer-Aided Analysis of Rigid and Flexible Mechanical Systems, Seabra Pereira M., Ambrósio, J. (eds.), Nato ASI Series, E-268, Kluwer Academic Publishers, pp. 501–529 (1994)
34. Bottasso, C.L., Bauchau, O.A., Cardona, A.: Time-step-size-independent conditioning and sensitivity to perturbations in the numerical solution of index three differential algebraic equations. SIAM J. Sci. Comput., to appear.